# Magnetic Field Induced Semimetal-to-Canted-Antiferromagnet Transition on the Honeycomb Lattice

Diplomarbeit

von

Martin Helmut Bercx

vorgelegt bei

Professor Dr. F. F. Assaad

Institut für Theoretische Physik und Astrophysik
Julius-Maximilians-Universität
Würzburg

14. April 2008

# Contents

# 1 Introduction

The study of systems with reduced dimensionality has been revitalized by the recent realization of graphene sheets. Since then graphene has triggered intensive research equally on the theoretical and experimental sides [28]. The spectrum of scientific research ranges from studies of BCS-BEC crossover of the attractive Hubbard model [11] to the very recent discovery of giant intrinsic carrier mobilities in single and bilayer graphene [10].
To form graphene carbon atoms crystallize in the honeycomb lattice. The electrons interact with the resulting periodic potential and display an unprecedented low energy behaviour. The excitations satisfy the massless Dirac equation as opposed to the Schrödinger equation which usually describes the electronic properties of materials. These massless Dirac fermions allow for several analogies with QED. As a consequence of the bipartite nature of the honeycomb lattice one may introduce a spin index called pseudospin to discriminate between the sublattices and evoke the concept of chirality [32].
Although the role of many-body interactions in graphene remains unclear so far modifications of the band structure which cannot be explained in terms of a single electron picture have been found. The observed kinks near the Fermi energy were atrributed to electron-phonon and elctron-plasmon interactions [29].
In this thesis the Hubbard model on the honeycomb lattice in an external magnetic field is studied. The tight-binding band diplays two inequivalent cone shaped singularities, the so called Dirac points which are located in the Brillouin zone where upper and lower band touch each other (Fig. 1.1). Consequently, in the honeycomb lattice at half filling the Fermi surface geometry is pointlike and the Fermi surface density of states vanishes linearly. A spin density wave instability according to the Stoner criterion therefore does not develop in the honeycomb lattice at an infinitesimally small $U$. It has been shown that the symnetry breaking phase transtions occurs at a finite $U_c$ and coincides with a Mott-Hubbard transition [13].
Introducing a magnetic field changes the Fermi surface geometry towards a circular-like shape and generates a finite density of states at the Fermi level. Nesting between up and down spin Fermi surface leads to a Stoner like instability towards canted antiferromagnetic order.
Since the Stoner criterion is a mean-field result a saddle point approximation should capture much of the underlying physics. We use this approach as a starting point. Treating the electron-electron interaction correctly with numerical quantum Monte Carlo simula-

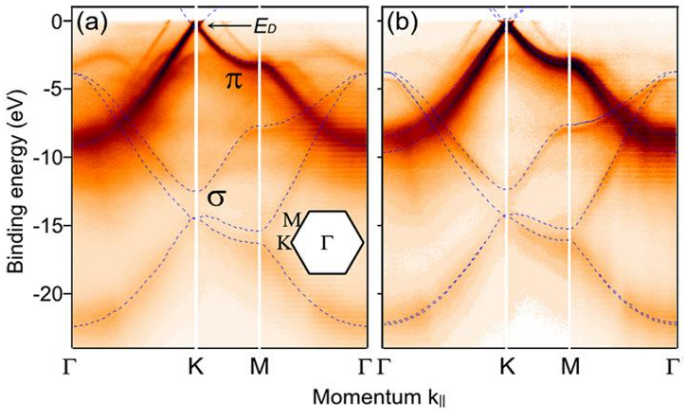


**Figure 1.1:** Photoemission intensity pattern of single (a) and bilayer (b) graphene along the high symmetry direction Γ-$K$-$M$-Γ which reflects its band structure. The dashed blue lines have been included for comparison with a density functional calculation. The figure is taken from [12].

tions this picture is confirmed to a good degree. A critical $U$ of order $U_c \approx 4-5$ is observed in accordance with what has been found out previously [13]. We show that under the action of the field the critical $U$ is lowered from the strong interaction of the free system towards an experimentally more accesible region. The transition takes the semimetal to an canted antiferromagnet which is heralded by the opening of a gap in the excitation spectrum.

The thesis is organized as follows. In chapter one the model Hamiltonian is introduced and is studied on a mean field level. By studying the transverse susceptibility we show that under the action of a vertical magnetic field the system gets logarithmically instable. This chapter concludes with the evaluation of the single-particle spectral function and the concomitant density of states. The chapters two and three are rather technical and include the foundations for the numerical treatment of the many-body problem. The quantum Monte Carlo approach, more precisely the projector quantum Monte Carlo algorithm, is explained and big emphasize lies on the stable computation of observables. Finally, in chapter four the numerically obtained static and dynamic results which include the staggered magnetization and the excitation spectra are discussed.

# 2 Mean Field Treatment

The standard model to describe the electronic and magnetic properties of correlated electrons on a lattice is the Hubbard model. Being conceptually simple this model incorporates two opposing trends: electron hopping which tends to delocalize the electrons and electron-electron interactions leading to localization. In this chapter the hexagonal lattice is discussed in the context of the Hubbard model.
The complexity of many particle problems can be dramatically reduced by a molecular field approximation. This approximation replaces the electron-electron interaction term in the Hamiltonian with effective one body expressions, thereby neglecting fluctuations of the particle operators. The idea is that fluctuations only play the role of small oscillations around the mean value of a physical observable. Given this simplification the interaction acts like a space and spin dependent external field, the molecular field. The molecular field is the one which minimizes the free energy. The problem is thus tractable on a mean field level, that is one may diagonalize the Hamiltonian and describe phase transitions. The prize we have to pay is the loss of information since effects governed by real electron correlations are lost. On the other hand the physical significance of the mean field solution is limited, since the assumptions needed to decouple the interaction term essentially are reconfirmed in the end. Nevertheless the mean field treatment serves a valuable starting point for more detailed analytical techniques or numerical approaches like the Quantum Monte Carlo method. The molecular field method is a self-consistent approximation and helps to understand fundamental properties of the hexagonal lattice. It is used to qualitatively describe the paramagnetic and antiferromagnetic phase and to extract the single particle spectral function.

## 2.1 The model Hamiltonian

The generic Hamilton operator in the Hubbard model is

$$H = H_T + H_I = -\sum_{i,j,\sigma}(t_{i,j} - \mu)\hat{c}^\dagger_{i,\sigma}\hat{c}_{j,\sigma} + U\sum_i \hat{n}_{i,\uparrow}\hat{n}_{i,\downarrow} \; . \tag{2.1}$$

Here $t_{i,j}$ are hopping integrals, $U$ is the on-site repulsion, $\mu$ is the chemical potential and $\hat{n}_{i,\sigma} = \hat{c}^\dagger_{i,\sigma}\hat{c}_{i,\sigma}$ is the electron density operator. In the following we assume strongly localized Wannier orbitals that we restrict ourselves to hopping processes to the nearest

neighbours, with $t_{i,j} \equiv t$. In the case of half-filling $\mu = 0$.
The lattice vectors are

$$\mathbf{a}_1 = a \begin{pmatrix} 1/2 \\ \sqrt{3}/2 \end{pmatrix} \qquad \mathbf{a}_2 = a \begin{pmatrix} 1 \\ 0 \end{pmatrix} \ , \tag{2.2}$$

$a$ is the distance of neighbouring sites on sublattice $A$ and $B$. The term of kinetic energy contains the hopping processes on the bipartite lattice and it reads

$$\begin{aligned} H_T &= -t \sum_{\mathbf{R},\,\sigma,\,\hat{a}\in A,\,\hat{b}\in B} (\hat{a}^\dagger_{\mathbf{R},\sigma}\hat{b}_{\mathbf{R},\sigma} + \hat{a}^\dagger_{\mathbf{R},\sigma}\hat{b}_{\mathbf{R}+\mathbf{a}_2-\mathbf{a}_1,\sigma} + \hat{a}^\dagger_{\mathbf{R},\sigma}\hat{b}_{\mathbf{R}-\mathbf{a}_1,\sigma}) + h.c. \\ &= -t \sum_{\mathbf{k},\sigma} \begin{pmatrix} \hat{a}^\dagger_{\mathbf{k},\sigma} & \hat{b}^\dagger_{\mathbf{k},\sigma} \end{pmatrix} \begin{bmatrix} H_{11} & H_{12} \\ H_{21} & H_{22} \end{bmatrix} \begin{pmatrix} \hat{a}_{\mathbf{k},\sigma} \\ \hat{b}_{\mathbf{k},\sigma} \end{pmatrix} \ , \end{aligned} \tag{2.3}$$

with

$$\begin{aligned} H_{11} &= H_{22} = 0 \\ H_{12} &= H^*_{21} = 1 + e^{\imath\mathbf{k}(\mathbf{a}_2-\mathbf{a}_1)} + e^{-\imath\mathbf{k}\mathbf{a}_1} \end{aligned} \tag{2.4}$$

Upon diagonalization of the Hermitian Hamilton matrix one gets the two tight binding bands[1] (Fig. 2.1)

$$\Gamma_\pm(\mathbf{k}) = \pm\sqrt{3 + 2\cos\mathbf{k}(\mathbf{a}_2 - \mathbf{a}_1) + 2\cos\mathbf{k}\mathbf{a}_1 + 2\cos\mathbf{k}\mathbf{a}_2} \quad . \tag{2.5}$$

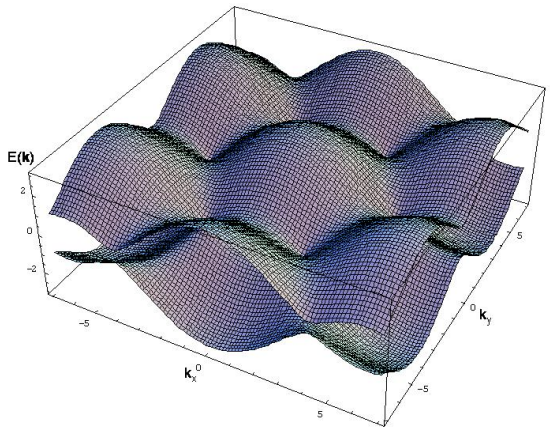


**Figure 2.1:** Energy spectrum $\Gamma(k_x, k_y)$ of the two dim. hexagonal lattice, based on the assumption of free electrons (tight-binding model). Valence and conduction band touch each other at the so-called Dirac points and the energy gap vanishes.

[1] Here and in the following we set $t \equiv 1$.

## 2.2 Examination of the transversal susceptibility

In this section we concentrate on possible magnetic instabilities of the free Hamiltonian under the action of a vertical magnetic field (conventionally chosen as $\mathbf{B} = B\mathbf{e}_z$), $H = H_T + H_{field}$. Magnetic order is heralded by the divergence of the appropriate magnetic susceptibility when the temperature goes to zero. Here we look at the possibility of staggered antiferromagnetic order in the transversal plane of the lattice.
The Hamiltonian can easily be diagonalized to

$$\begin{aligned} H &= H_T + \frac{B}{2}\sum_{A,B}\sum_{\mathbf{k},\sigma} p_\sigma \hat{n}_\sigma \\ &= \sum_{\mathbf{k},\sigma} E_\gamma\,(\mathbf{k},\sigma)\hat{\gamma}^\dagger\hat{\gamma} + E_\eta(\mathbf{k},\sigma)\,\hat{\eta}^\dagger\hat{\eta} \end{aligned} \tag{2.6}$$

The quasi particle energies[2] are $E_{\gamma,\eta}(\mathbf{k},\sigma) = \frac{B}{2}p_\sigma \mp \Gamma(\mathbf{k})$, $p_\sigma = \pm 1$, and the particle operators are

$$\begin{aligned} \hat{\gamma} &= \frac{1}{\sqrt{2}}\left(\hat{a} + \frac{\Gamma}{H_{21}}\hat{b}\right), \\ \hat{\eta} &= \frac{1}{\sqrt{2}}\left(\frac{-\Gamma}{H_{12}}\hat{a} + \hat{b}\right), \\ \hat{a} &= \frac{1}{\sqrt{2}}\left(\hat{\gamma} - \frac{\Gamma}{H_{21}}\hat{\eta}\right), \\ \hat{b} &= \frac{1}{\sqrt{2}}\left(\frac{\Gamma}{H_{12}}\hat{\gamma} + \hat{\eta}\right). \end{aligned} \tag{2.7}$$

Correlation functions like the single particle Green function or the susceptibility are $2\times 2$ matrices as a consequence of the two sublattices used to describe the hexagonal lattice. In particular the tensorial nature of the transversal spin susceptibility $\chi^{+-}$ lies in the two orbitals per unit cell and is not due to anisotropy effects. The tensor of the transversal susceptibility is:

$$\chi^{+-}(\mathbf{q},\omega) = \begin{pmatrix} \chi^{+-}_{AA} & \chi^{+-}_{AB} \\ \chi^{+-}_{BA} & \chi^{+-}_{BB} \end{pmatrix} \tag{2.8}$$

From now on we are only concerned with the static case, $\chi^{+-}(\mathbf{q}) \equiv \chi^{+-}(\mathbf{q},\omega=0)$. Within the Matsubara formalism[3] the components are defined as

$$\chi^{+-}_{\mu,\nu}(\mathbf{q}) = \int_0^\beta d\tau \langle S^+_\mu(\mathbf{q},\tau) S^-_\nu(\text{-}\mathbf{q},0)\rangle\ . \tag{2.9}$$

[2] Here, $\Gamma \equiv \Gamma_+$.

[3] In this work, the modified Heisenberg picture is employed to describe the time evolution in imaginary time, that is $A(\tau) = e^{H\tau}A(0)e^{-H\tau}$. [1],[3]. For notational clarity, we have set $\hbar \equiv 1$ in the whole text.

The indices are $\mu = A, B,\ \nu = A, B$ and the spin raising and lowering operators are

$$S_\mu^{+(-)}(\mathbf{q}) = \frac{1}{\sqrt{N}} \sum_{\mathbf{k}} \hat{c}^\dagger_{\mu_{\mathbf{k},\uparrow(\downarrow)}} \hat{c}_{\mu_{\mathbf{k}+\mathbf{q},\downarrow(\uparrow)}} \ , \tag{2.10}$$

with the particle operators $\hat{c}_A = \hat{a}$, $\hat{c}_B = \hat{b}$ on the sublattices. For later use we note that $\chi^{+-}_{\mu,\mu} = \chi^{+-}_{\nu,\nu}$ and $\chi^{+-}_{\mu,\nu} = (\chi^{+-}_{\nu,\mu})^*$, in the static ($\omega = 0$) case $\chi^{+-}_{\mu,\nu} = \chi^{+-}_{\nu,\mu}$. The transversal magnetization on orbital $\mu$ amounts to

$$m^{xy}_\mu = \sum_{\alpha=\mu,\nu} \chi^{+-}_{\mu,\alpha} B^{xy}_\alpha \ . \tag{2.11}$$

$B^{xy}_\alpha$ are the orbital components of a transversal magnetic field. For $B^{xy}_\mu = -B^{xy}_\nu$ we obtain the antiferromagnetic susceptibility $\chi^{+-}_{\mu\mu} - \chi^{+-}_{\mu\nu}$, for $B^{xy}_\mu = B^{xy}_\nu$ the ferromagnetic susceptibility $\chi^{+-}_{\mu\mu} + \chi^{+-}_{\mu\nu}$. Since the ordering takes places within the orbitals at formally the same lattice point it can be characterized with the wave vector $\mathbf{q} = 0$. However, for reasons of generality we keep the vector $\mathbf{q}$ during the calculation and in the end we set it equal to zero.
The components $\chi^{+-}_{\mu,\nu}(\mathbf{q})$ may be calculated applying Wick's theorem and using the quasiparticle expressions for $\hat{\gamma}$ und $\hat{\eta}$ (2.7):

$$\begin{aligned}
\chi^{+-}_{\mu,\nu}(\mathbf{q}) &= \int_0^\beta d\tau \langle S^+_\mu(\mathbf{q},\tau) S^-_\nu(-\mathbf{q},0)\rangle \\
&= \frac{1}{N}\int_0^\beta d\tau \sum_{\mathbf{k},\mathbf{k\prime}} \langle \hat{c}^\dagger_{\mu_{\mathbf{k},\uparrow}}(\tau) \hat{c}_{\mu_{\mathbf{k}+\mathbf{q},\downarrow}}(\tau) \hat{c}^\dagger_{\nu_{\mathbf{k\prime},\downarrow}}(0) \hat{c}_{\nu_{\mathbf{k\prime}-\mathbf{q},\uparrow}}(0)\rangle \\
&= \frac{1}{N}\int_0^\beta d\tau \sum_{\mathbf{k},\mathbf{k\prime}} \langle \hat{c}^\dagger_{\mu_{\mathbf{k},\uparrow}}(\tau) \hat{c}_{\mu_{\mathbf{k}+\mathbf{q},\downarrow}}(\tau)\rangle \langle \hat{c}^\dagger_{\nu_{\mathbf{k\prime},\downarrow}}(0) \hat{c}_{\nu_{\mathbf{k\prime}-\mathbf{q},\uparrow}}(0)\rangle \\
&\quad + \langle \hat{c}^\dagger_{\mu_{\mathbf{k},\uparrow}}(\tau) \hat{c}_{\nu_{\mathbf{k\prime}-\mathbf{q},\uparrow}}(0)\rangle \langle \hat{c}_{\mu_{\mathbf{k}+\mathbf{q},\downarrow}}(\tau) \hat{c}^\dagger_{\nu_{\mathbf{k\prime},\downarrow}}(0)\rangle \\
&= \frac{1}{N}\int_0^\beta d\tau \sum_{\mathbf{k}} \langle \hat{c}^\dagger_{\mu_{\mathbf{k},\uparrow}}(\tau) \hat{c}_{\nu_{\mathbf{k},\uparrow}}(0)\rangle \langle \hat{c}_{\mu_{\mathbf{k}+\mathbf{q},\downarrow}}(\tau) \hat{c}^\dagger_{\nu_{\mathbf{k}+\mathbf{q},\downarrow}}(0)\rangle \\
&= \frac{1}{4N}\int_0^\beta d\tau \sum_{\mathbf{k}} \Big( \langle \hat{\gamma}^\dagger(\tau)\hat{\gamma}(0)\rangle_{\mathbf{k},\uparrow} \pm \langle \hat{\eta}^\dagger(\tau)\hat{\eta}(0)\rangle_{\mathbf{k},\uparrow} \Big) \Big( \langle \hat{\gamma}(\tau)\hat{\gamma}^\dagger(0)\rangle_{\mathbf{k}+\mathbf{q},\downarrow} \pm \langle \hat{\eta}(\tau)\hat{\eta}^\dagger(0)\rangle_{\mathbf{k}+\mathbf{q},\downarrow} \Big) \\
&= \frac{1}{4N}\int_0^\beta d\tau \sum_{\mathbf{k}} \Big[ \langle \hat{\gamma}^\dagger(\tau)\hat{\gamma}(0)\rangle_{\mathbf{k},\uparrow} \langle \hat{\gamma}(\tau)\hat{\gamma}^\dagger(0)\rangle_{\mathbf{k}+\mathbf{q},\downarrow} \pm \langle \hat{\gamma}^\dagger(\tau)\hat{\gamma}(0)\rangle_{\mathbf{k},\uparrow} \langle \hat{\eta}(\tau)\hat{\eta}^\dagger(0)\rangle_{\mathbf{k}+\mathbf{q},\downarrow} \\
&\quad \pm \langle \hat{\eta}^\dagger(\tau)\hat{\eta}(0)\rangle_{\mathbf{k},\uparrow} \langle \hat{\gamma}(\tau)\hat{\gamma}^\dagger(0)\rangle_{\mathbf{k}+\mathbf{q},\downarrow} + \langle \hat{\eta}^\dagger(\tau)\hat{\eta}(0)\rangle_{\mathbf{k},\uparrow} \langle \hat{\eta}(\tau)\hat{\eta}^\dagger(0)\rangle_{\mathbf{k}+\mathbf{q},\downarrow} \Big] \ .
\end{aligned} \tag{2.12}$$

Here, "+" stands for $\mu = \nu$ and $-$" for $\mu \neq \nu$; the first term in line three is equal to zero since the Hamiltonian (2.6) does not include spin flip processes. The antiferromagnetic

and ferromagnetic susceptibilities are therefore written as

$$\chi^{+-}_{\mu\mu} - \chi^{+-}_{\mu\nu} \tag{2.13}$$
$$= \frac{1}{2N}\int_0^\beta d\tau \sum_{\mathbf{k}} \left( \langle \hat{\gamma}^\dagger(\tau)\hat{\gamma}(0)\rangle_{\mathbf{k},\uparrow} \langle \hat{\eta}(\tau)\hat{\eta}^\dagger(0)\rangle_{\mathbf{k}+\mathbf{q},\downarrow} + \langle \hat{\eta}^\dagger(\tau)\hat{\eta}(0)\rangle_{\mathbf{k},\uparrow} \langle \hat{\gamma}(\tau)\hat{\gamma}^\dagger(0)\rangle_{\mathbf{k}+\mathbf{q},\downarrow} \right)$$
$$\chi^{+-}_{\mu\mu} + \chi^{+-}_{\mu\nu} \tag{2.14}$$
$$= \frac{1}{2N}\int_0^\beta d\tau \sum_{\mathbf{k}} \left( \langle \hat{\gamma}^\dagger(\tau)\hat{\gamma}(0)\rangle_{\mathbf{k},\uparrow} \langle \hat{\gamma}(\tau)\hat{\gamma}^\dagger(0)\rangle_{\mathbf{k}+\mathbf{q},\downarrow} + \langle \hat{\eta}^\dagger(\tau)\hat{\eta}(0)\rangle_{\mathbf{k},\uparrow} \langle \hat{\eta}(\tau)\hat{\eta}^\dagger(0)\rangle_{\mathbf{k}+\mathbf{q},\downarrow} \right) .$$

We proceed to calculate the ferromagnetic susceptibility, introducing the short notation $\hat{c}_i$ with $i = \gamma, \eta$ referring to the $\hat{\gamma}$ and $\hat{\eta}$ operators.

$$\begin{aligned}
\chi^{+-}_{\mu\mu} + \chi^{+-}_{\mu\nu} &= \frac{1}{2N}\int_0^\beta d\tau \sum_{\mathbf{k}} \sum_{i=\gamma,\eta} \langle \hat{c}_i^\dagger(\tau)\hat{c}_i(0)\rangle_{\mathbf{k},\uparrow} \langle \hat{c}_i(\tau)\hat{c}_i^\dagger(0)\rangle_{\mathbf{k}+\mathbf{q},\downarrow} \\
&= \frac{1}{2N}\int_0^\beta d\tau \sum_{\mathbf{k}} \sum_{i=\gamma,\eta} e^{\tau\left(E_i(\mathbf{k},\uparrow) - E_i(\mathbf{k}+\mathbf{q},\downarrow)\right)} \langle \hat{c}_i^\dagger\hat{c}_i\rangle_{\mathbf{k},\uparrow} \left(1 - \langle \hat{c}_i^\dagger\hat{c}_i\rangle_{\mathbf{k}+\mathbf{q},\downarrow}\right) \\
&= \frac{1}{2N}\sum_{\mathbf{k}} \sum_{i=\gamma,\eta} \frac{e^{\beta\left(E_i(\mathbf{k},\uparrow) - E_i(\mathbf{k}+\mathbf{q},\downarrow)\right)} - 1}{E_i(\mathbf{k},\uparrow) - E_i(\mathbf{k}+\mathbf{q},\downarrow)} \langle \hat{c}_i^\dagger\hat{c}_i\rangle_{\mathbf{k},\uparrow} e^{\beta E_i(\mathbf{k}+\mathbf{q},\downarrow)} \langle \hat{c}_i^\dagger\hat{c}_i\rangle_{\mathbf{k}+\mathbf{q},\downarrow} \\
&= \frac{1}{2N}\sum_{\mathbf{k}} \sum_{i=\gamma,\eta} \frac{f_i(\mathbf{k}+\mathbf{q},\downarrow) - f_i(\mathbf{k},\uparrow)}{E_i(\mathbf{k},\uparrow) - E_i(\mathbf{k}+\mathbf{q},\downarrow)} \\
&\overset{\mathbf{q}=0}{=} \frac{1}{2N}\sum_{\mathbf{k}} \sum_{i=\gamma,\eta} \underbrace{\frac{f_i(\mathbf{k},\downarrow) - f_i(\mathbf{k},\uparrow)}{E_i(\mathbf{k},\uparrow) - E_i(\mathbf{k},\downarrow)}}_{B} \\
&= \frac{1}{2NB}\sum_{\mathbf{k}} \sum_{i=\gamma,\eta} \left(f_i(\mathbf{k},\downarrow) - f_i(\mathbf{k},\uparrow)\right)
\end{aligned} \tag{2.15}$$

In line four the Fermi function $f_i(\mathbf{k}) = \frac{1}{e^{\beta E_i(\mathbf{k})}+1}$ and $E_i(\mathbf{k}) = p_\sigma \frac{B}{2} + \Gamma_i$ was introduced. The parenthesis in the last line denote the magnetization in $z$-direction for both bands $j = \gamma, \eta$. This expression is zero for vanishing external field and at a given field it approaches unity for $T \to 0$ (Fig.2.2).

We now evaluate the antiferromagnetic susceptibility, again using the notation $\hat{c}_i, i = \gamma, \eta$.

$$\begin{aligned}
\chi^{+-}_{\mu\mu} - \chi^{+-}_{\mu\nu} &= \frac{1}{2N}\int_0^\beta d\tau \sum_{\mathbf{k}} \sum_{\substack{i=\gamma,\eta \\ j=\gamma,\eta \\ i\neq j}} \langle \hat{c}_i^\dagger(\tau)\hat{c}_i(0)\rangle_{\mathbf{k},\uparrow} \langle \hat{c}_j(\tau)\hat{c}_j^\dagger(0)\rangle_{\mathbf{k}+\mathbf{q},\downarrow} \\
&= \frac{1}{2N}\int_0^\beta d\tau \sum_{\mathbf{k}} \sum_{\substack{i=\gamma,\eta \\ j=\gamma,\eta \\ i\neq j}} e^{\tau\left(E_i(\mathbf{k},\uparrow) - E_j(\mathbf{k}+\mathbf{q},\downarrow)\right)} \langle \hat{c}_i^\dagger \hat{c}_i\rangle_{\mathbf{k},\uparrow} \left(1 - \langle \hat{c}_j^\dagger \hat{c}_j\rangle_{\mathbf{k}+\mathbf{q},\downarrow}\right) \\
&= \frac{1}{2N}\sum_{\mathbf{k}} \sum_{\substack{i=\gamma,\eta \\ j=\gamma,\eta \\ i\neq j}} \frac{e^{\beta\left(E_i(\mathbf{k},\uparrow) - E_j(\mathbf{k}+\mathbf{q},\downarrow)\right)} - 1}{E_i(\mathbf{k},\uparrow) - E_j(\mathbf{k}+\mathbf{q},\downarrow)} \langle \hat{c}_i^\dagger \hat{c}_i\rangle_{\mathbf{k},\uparrow} e^{\beta E_j(\mathbf{k}+\mathbf{q},\downarrow)} \langle \hat{c}_j^\dagger \hat{c}_j\rangle_{\mathbf{k}+\mathbf{q},\downarrow} \\
&= \frac{1}{2N}\sum_{\mathbf{k}} \sum_{\substack{i=\gamma,\eta \\ j=\gamma,\eta \\ i\neq j}} \frac{f_j(\mathbf{k}+\mathbf{q},\downarrow) - f_i(\mathbf{k},\uparrow)}{E_i(\mathbf{k},\uparrow) - E_j(\mathbf{k}+\mathbf{q},\downarrow)} \\
&\overset{\mathbf{q}=0}{=} \frac{1}{2N}\sum_{\mathbf{k}} \sum_{\substack{i=\gamma,\eta \\ j=\gamma,\eta \\ i\neq j}} \frac{f_j(\mathbf{k},\downarrow) - f_i(\mathbf{k},\uparrow)}{E_i(\mathbf{k},\uparrow) - E_j(\mathbf{k},\downarrow)} \, . \qquad (2.16)
\end{aligned}$$

The denominator can be written as

$$E_i(\mathbf{k},\uparrow) - E_j(\mathbf{k},\downarrow) = \frac{B}{2} + \Gamma_i - \left(-\frac{B}{2} + \Gamma_j\right) = B + \Gamma_i - \Gamma_j = B - 2\Gamma_j = 2\left(\frac{B}{2} - \Gamma_j\right) , \qquad (2.17)$$

since $\Gamma_j = -\Gamma, +\Gamma$ for $j = \gamma, \eta$. The enumerator is

$$\begin{aligned}
f_j(\mathbf{k},\downarrow) - f_i(\mathbf{k},\uparrow) &= \frac{1}{e^{\beta\left(-\frac{B}{2}+\Gamma_j\right)}+1} - \frac{1}{e^{\beta\left(\frac{B}{2}+\Gamma_i\right)}+1} \qquad (2.18) \\
&\overset{\Gamma_i=-\Gamma_j}{=} \frac{e^{-\beta\left(-\frac{B}{2}+\Gamma_j\right)}}{1+e^{-\beta\left(-\frac{B}{2}+\Gamma_j\right)}} - \frac{1}{e^{-\beta\left(-\frac{B}{2}+\Gamma_j\right)}+1} \\
&= \frac{e^{-\beta\left(-\frac{B}{2}+\Gamma_j\right)} - 1}{1+e^{-\beta\left(-\frac{B}{2}+\Gamma_j\right)}} = \tanh\left(\frac{\beta}{2}\left(\frac{B}{2} - \Gamma_j\right)\right) \, .
\end{aligned}$$

We finally get with $\xi_j = \frac{B}{2} - \Gamma_j$

$$\begin{aligned}
\chi^{+-}_{\mu\mu} - \chi^{+-}_{\mu\nu} &= \frac{1}{2}\frac{1}{N}\sum_{\mathbf{k}} \sum_{j=\gamma,\eta} \frac{1}{2\left(\frac{B}{2} - \Gamma_j\right)} \tanh\left(\frac{\beta}{2}\left(\frac{B}{2} - \Gamma_j\right)\right) \\
&= \frac{1}{2}\frac{1}{N}\sum_{\mathbf{k}} \sum_{j=\gamma,\eta} \frac{1}{2\xi_j} \tanh\left(\frac{\beta}{2}\left(\xi_j\right)\right) \, . \qquad (2.19)
\end{aligned}$$

Using the approximation (in the appendix) for $\tanh\left(\frac{\beta}{2}\left(\xi_j\right)\right)$,

$$\left(\chi^{+-}_{\mu\mu} - \chi^{+-}_{\mu\nu}\right)(T) \approx \frac{1}{2}\sum_{j=\gamma,\eta} DOS(\epsilon_{F,j}) \, \ln\left(\frac{W}{2T}\right) . \qquad (2.20)$$

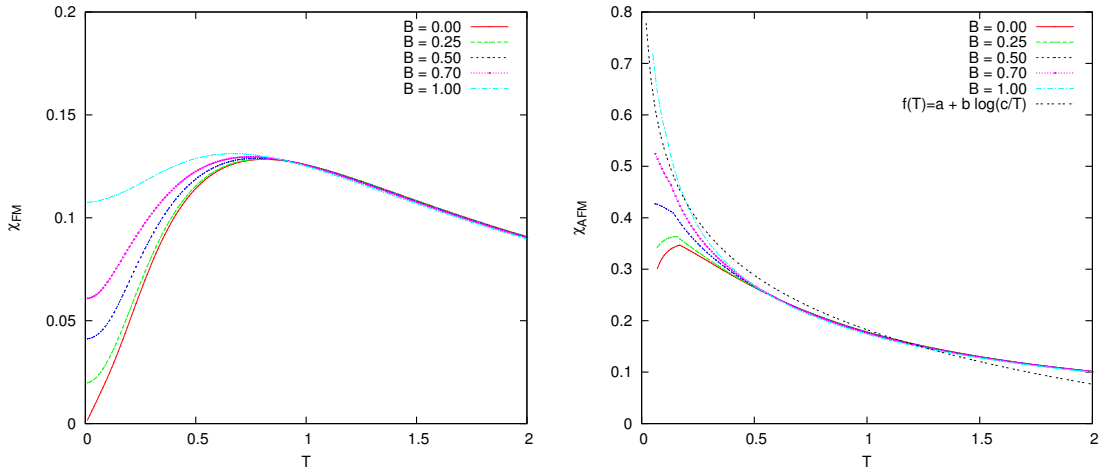


(a) $\left(\chi^{+-}_{\mu\mu} + \chi^{+-}_{\mu\nu}\right)(T)$ (b) $\left(\chi^{+-}_{\mu\mu} - \chi^{+-}_{\mu\nu}\right)(T)$

**Figure 2.2:** Numerical evaluation of the ferromagnetic and antiferromagnetic susceptibility, for varying fields $B$. The logarithmic divergence of $\chi^{+-}_{AFM}(T)$ as $T \to 0$ is visualized by a logarithmic fitting function $f(T)$ $(a = 0.27, b = 0.15, c = 0.5)$.

Thus, $\left(\chi^{+-}_{\mu\mu} - \chi^{+-}_{\mu\nu}\right)(T)$ diverges logarithmically as $T$ goes to zero. (Fig.2.2) This behaviour is signaled already in the Lindhard type result for the antiferromagnetic susceptibility, (2.16). We consider the nesting condition, which is known to be

$$\epsilon(\mathbf{k} + \mathbf{Q}_{nest}) = -\epsilon(\mathbf{k}) \; . \tag{2.21}$$

In our case antiferromagnetic order sets in at $\mathbf{Q}_{nest} = 0$ so the nesting condition now reads

$$E_i(\mathbf{k}, \uparrow) = -E_j(\mathbf{k}, \downarrow) \tag{2.22}$$

which is obviously fulfilled. That is, we describe the hexagonal lattice being on the edge of staggered antiferromagnetic order as a consequence of the nesting of its up and down Fermisurface. The ordering is predicted to occur at a small non-zero interaction $U$ (see section 2.4).

## 2.3 Mean field decoupling

We now consider the following Hubbard model with on-site interaction and external magnetic field:

$$\begin{aligned} H &= H_{hopping} + H_{field} + H_I \\ &= -t \sum_{\mathbf{k},\sigma} \left[ \left(1 + e^{\imath \mathbf{k}(\mathbf{a}_2 - \mathbf{a}_1)} + e^{-\imath \mathbf{k} \mathbf{a}_1}\right) \hat{a}^\dagger_{\mathbf{k},\sigma} \hat{b}_{\mathbf{k},\sigma} + \left(1 + e^{-\imath \mathbf{k}(\mathbf{a}_2 - \mathbf{a}_1)} + e^{\imath \mathbf{k} \mathbf{a}_1}\right) \hat{b}^\dagger_{\mathbf{k},\sigma} \hat{a}_{\mathbf{k},\sigma} \right] \\ &+ \frac{B}{2} \sum_{A,B} \sum_{\mathbf{k},\sigma} p_\sigma \hat{n}_\sigma + U \sum_{A,B} \sum_i \left(\hat{n}_{i\uparrow} - \frac{1}{2}\right)\left(\hat{n}_{i\downarrow} - \frac{1}{2}\right) \; . \end{aligned} \tag{2.23}$$

In order to arrive at an effective molecular field Hamiltonian we make two assumptions:

1. The biquadratic term is rewritten as:

$$\begin{aligned} H_I &= U \sum_{A,B} \sum_i \left(\hat{n}_{i\uparrow} - \frac{1}{2}\right)\left(\hat{n}_{i\downarrow} - \frac{1}{2}\right) = -\frac{U}{2} \sum_{A,B} \sum_i \left[(\hat{n}_{i,\uparrow} - \hat{n}_{i,\downarrow})^2 - 1\right] \\ &= -\frac{U}{2} \sum_{A,B} \sum_i \left[(2\hat{S}^z_{i,\alpha})^2 - 1\right] = -\frac{2}{3} U \sum_{A,B} \sum_i \left(\hat{S}_{i,\alpha}\right)^2 + UN \; . \end{aligned} \tag{2.24}$$

   In this notation the spin-rotational invariance, that is the invariance of $H_I$ under simultaneous rotation of all spins is explicitely used.

2. The transversal component $m_x$ of the magnetization $\vec{m}$ is assumed to be staggered, that is alternating on the sublattices $A$ and $B$: $m_{x,A} = -m_{x,B}$. Put differently, with the index $\alpha = 0, 1$ which labels the orbitals in the unit cell:

$$\vec{m}_\alpha = \Big(m_x(-1)^\alpha, \quad 0, \quad m_z\Big) \tag{2.25}$$

   .

Therefore we assume the magnetization $\vec{m}$ to have a constant component $m_z$ parallel to the field axis and a staggered component $m_x(-1)^\alpha$ in the $xy$-plane perpendicular to the field. This breaks the spin-rotational invariance. The components $m_x$ and $m_y$ make up the molecular field in this case. To approximate $H_I$ we employ the notation:

$$\begin{aligned} \vec{S}_{i,\alpha} &= \vec{m}_\alpha + (\vec{S}_{i,\alpha} - \vec{m}_\alpha) \\ \hat{S}^2_{i,\alpha} &= 2m_x(-1)^\alpha \, \hat{S}^x_{i,\alpha} + 2m_z \, \hat{S}^z_{i,\alpha} - m_x^2 - m_z^2 + \underbrace{(\vec{S}_{i,\alpha} - \vec{m}_\alpha)^2}_{fluctuations} \; . \end{aligned} \tag{2.26}$$

By inserting in (2.24) one obtains the mean-field approximation, neglecting the fluctuations:

$$\begin{aligned} H_{I,MF} &= \frac{2}{3} U \sum_{\mathbf{k}} [m_x(\hat{a}^\dagger_{\mathbf{k}\uparrow}\hat{a}_{\mathbf{k}\downarrow} + \hat{a}^\dagger_{\mathbf{k}\downarrow}\hat{a}_{\mathbf{k}\uparrow}) - m_z(\hat{a}^\dagger_{\mathbf{k}\uparrow}\hat{a}_{\mathbf{k}\uparrow} - \hat{a}^\dagger_{\mathbf{k}\downarrow}\hat{a}_{\mathbf{k}\downarrow}) \\ &- m_x(\hat{b}^\dagger_{\mathbf{k}\uparrow}\hat{b}_{\mathbf{k}\downarrow} + \hat{b}^\dagger_{\mathbf{k}\downarrow}\hat{b}_{\mathbf{k}\uparrow}) - m_z(\hat{b}^\dagger_{\mathbf{k}\uparrow}\hat{b}_{\mathbf{k}\uparrow} - \hat{b}^\dagger_{\mathbf{k}\downarrow}\hat{b}_{\mathbf{k}\downarrow}) + 2m_x^2 + 2m_z^2] + UN \; . \end{aligned} \tag{2.27}$$

The mean-field Hamiltonian $H_{MF}$ is bilinear in the fermion operators:

$$\begin{aligned} H_{MF} &= \sum_{\mathbf{k},\sigma} -t(\cdots)\, \hat{a}^\dagger_{\mathbf{k},\sigma}\hat{b}_{\mathbf{k},\sigma} - t(\cdots)^* \, \hat{b}^\dagger_{\mathbf{k},\sigma}\hat{a}_{\mathbf{k},\sigma} \\ &+ \frac{B}{2}\mu_B p_\sigma(\hat{n}_a + \hat{n}_b) + \frac{2}{3}U\left[m_x(\hat{a}^\dagger_{\mathbf{k},\sigma}\hat{a}_{\mathbf{k},-\sigma} - \hat{b}^\dagger_{\mathbf{k},\sigma}\hat{b}_{\mathbf{k},-\sigma}) - m_z \, p_\sigma(\hat{n}^a_{\mathbf{k},\sigma} + \hat{n}^b_{\mathbf{k},\sigma})\right] \\ &+ \frac{4}{3}UN(m_x^2 + m_z^2) + UN \; , \end{aligned} \tag{2.28}$$

here $(\cdots)$,$(\cdots)^*$ are the hopping terms $H_{12}$,$H_{21}$ (2.4). Restated with the hermitian Hamilton matrix

$$H_{MF} =$$

$$\sum_{\mathbf{k}} \left(\hat{a}^\dagger_{\mathbf{k},\uparrow}, \hat{b}^\dagger_{\mathbf{k},\uparrow}, \hat{a}^\dagger_{\mathbf{k},\downarrow}, \hat{b}^\dagger_{\mathbf{k},\downarrow}\right) \begin{bmatrix} \left(\frac{B}{2} - \frac{2}{3}Um_z\right) & -t(\cdots) & \frac{2}{3}Um_x & 0 \\ -t(\cdots)^* & \left(\frac{B}{2} - \frac{2}{3}Um_z\right) & 0 & -\frac{2}{3}Um_x \\ \frac{2}{3}Um_x & 0 & \left(-\frac{B}{2} + \frac{2}{3}Um_z\right) & -t(\cdots) \\ 0 & -\frac{2}{3}Um_x & -t(\cdots)^* & \left(-\frac{B}{2} + \frac{2}{3}Um_z\right) \end{bmatrix} \begin{pmatrix} \hat{a}_{\mathbf{k},\uparrow} \\ \hat{b}_{\mathbf{k},\uparrow} \\ \hat{a}_{\mathbf{k},\downarrow} \\ \hat{b}_{\mathbf{k},\downarrow} \end{pmatrix}$$

$$+\frac{4}{3}UN(m_x^2 + m_z^2) + UN \; . \tag{2.29}$$

The Hamilton matrix can be brought to diagonal form with a unitary transformation $\mathbf{U}^\dagger\mathbf{U} = \mathbf{1}$. We define the quasiparticle operators

$$\hat{\gamma}^\dagger_n = \sum_m \hat{c}^\dagger_m \mathbf{U}^\dagger_{m,n}, \quad \hat{\gamma}_n = \sum_m \mathbf{U}_{n,m}\hat{c}_m \tag{2.30}$$

and

$$\hat{c}^\dagger_n = \sum_m \hat{\gamma}^\dagger_m \mathbf{U}_{m,n}, \quad \hat{c}_n = \sum_m \mathbf{U}^\dagger_{n,m}\hat{\gamma}_m \; . \tag{2.31}$$

The operators $\hat{c}_{1,2,3,4}$ stand for $\hat{a}_\uparrow, \hat{b}_\uparrow, \hat{a}_\downarrow, \hat{b}_\downarrow$. Thus

$$H_{MF} = \sum_{\mathbf{k}} \sum_{\eta=1,2,3,4} E_{\eta,\mathbf{k}} \; \hat{\gamma}^\dagger_{\eta,\mathbf{k}}\hat{\gamma}_{\eta,\mathbf{k}} \;\; + \;\; \frac{4}{3}UN(m_x^2 + m_z^2) + UN \; . \tag{2.32}$$

The four quasiparticle bands consist of two hole bands $E^h_{\eta,\mathbf{k}}$ and two particle bands $E^p_{\eta,\mathbf{k}}$,

$$E^{p,h}_{\eta,\mathbf{k}} = \pm\sqrt{\left(\frac{2}{3}Um_z - \frac{B}{2}\right)^2 + \left(\frac{2}{3}Um_x\right)^2 + \epsilon^2_{\mathbf{k}} \pm \left(B - \frac{4}{3}Um_z\right)\epsilon_{\mathbf{k}}} \; . \tag{2.33}$$

The free dispersion (2.5) is denoted as $\epsilon_{\mathbf{k}}$. In the ground state we assume that the hole bands are completely filled and the particle bands completely empty:

$$\begin{aligned} E_{gs} &= \sum_{\mathbf{k}} \left(E_{1,\mathbf{k}} + E_{2,\mathbf{k}}\right) \;\; + \;\; \frac{4}{3}UN(m_x^2 + m_z^2) + UN \\ &= -\sum_{\mathbf{k}} \sqrt{\left(\frac{2}{3}Um_z - \frac{B}{2}\right)^2 + \left(\frac{2}{3}Um_x\right)^2 + \epsilon^2_{\mathbf{k}} + \left(B - \frac{4}{3}Um_z\right)\epsilon_{\mathbf{k}}} \\ &+ \sqrt{\left(\frac{2}{3}Um_z - \frac{B}{2}\right)^2 + \left(\frac{2}{3}Um_x\right)^2 + \epsilon^2_{\mathbf{k}} - \left(B - \frac{4}{3}Um_z\right)\epsilon_{\mathbf{k}}} + \frac{4}{3}UN(m_x^2 + m_z^2) + UN \; . \end{aligned} \tag{2.34}$$

To determine the parameters $m_z$ and $m_x$ we understand them as variational parameters which minimize $E_{gs}(m_x, m_z)$. With this approach one arrives at the mean field equations (gap equations)

$$\begin{aligned} \frac{\partial E_{gs}\,(m_x, m_z)}{\partial m_x} &= 0 \\ \frac{\partial E_{gs}\,(m_x, m_z)}{\partial m_z} &= 0\,, \end{aligned} \tag{2.35}$$

or

$$\begin{aligned} m_x &= -\frac{1}{N}\sum_{\mathbf{k}} \left(\frac{1}{E_{1,\mathbf{k}}} + \frac{1}{E_{2,\mathbf{k}}}\right) \frac{1}{6} U m_x \\ m_z &= -\frac{1}{N}\sum_{\mathbf{k}} \left(\frac{1}{E_{1,\mathbf{k}}} + \frac{1}{E_{2,\mathbf{k}}}\right) \left(\frac{1}{6} U m_z - \frac{1}{8} B\right) - \left(\frac{1}{E_{1,\mathbf{k}}} - \frac{1}{E_{2,\mathbf{k}}}\right) \frac{\epsilon_{\mathbf{k}}}{4}\,. \end{aligned} \tag{2.36}$$

They may be solved numerically.

## 2.4 Meanfield phase transition

The reason to study many-particle systems is the search for correlation effects. By definition these are effects which cannot be described within an independent electron approximation [2]. Having introduced the explicit form (2.25) of the molecular field we already anticipated the spontaneous symmetry breaking. Therefore we know that the system will develop Neél order beyond a critical $U$ (for $H = 0$) and canted antiferromagetic order (for $H > 0$)[4]. Based on this qualitative considerations we expect a phase transition from paramagnetic to antiferromagnetic state at $U_c(H)$ which coincidences with a semi metal-insulator transition. In the context of the mean field approximation we call the insulating phase an antiferromagnetic Slater insulator. The hexagonal lattice is bipartite, that is it consists of two interpenetrating triangular lattices and in the antiferromagnetic phase an alternating order in the $xy$-plane is realized. The spin density wave is self-stabilizing and its wave vector $\mathbf{Q}$ is commensurate with the lattice. Since we describe the lattice according to a basis with two orbitals we get $\mathbf{Q} = (0, 0)$. Naturally this self-consistent band picture which predicts the insulating state as a consequence of electron exchange is too simple to explain a real Mott-Heisenberg transition. This would require a theory for correlated electrons.

The self-consistent solutions for $m_z$ and $m_x$ as a function of $H$ and $U$, as well as the total magnetization $m = \sqrt{m_x^2 + m_z^2}$ are shown in Fig.(2.4).

Based on the mean field approach we observe a critical interaction strength of $U_c \cong 4$. For $U > U_c$ there exists already at $H = 0$ a finite transversal magnetization that is a gap

[4]Following conventional notation, we denote the magnetic field with the paramter $H$ instead of $B$ from now on, since it cannot be mistaken with the Hamiltonian anymore.

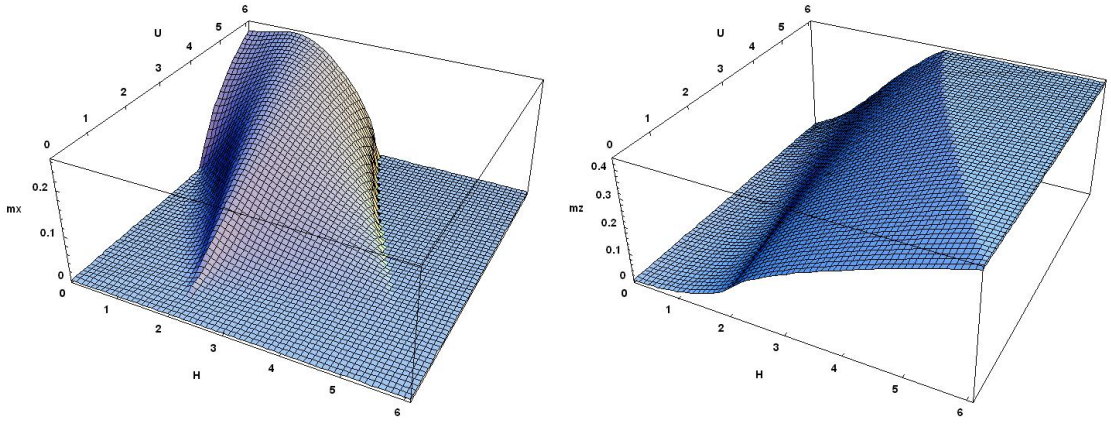


(a) $m_x$ (b) $m_z$

**Figure 2.3:** Components of the magnetization as a function of $H$ and $U$, resulting from numerical solution of the mean field equations.

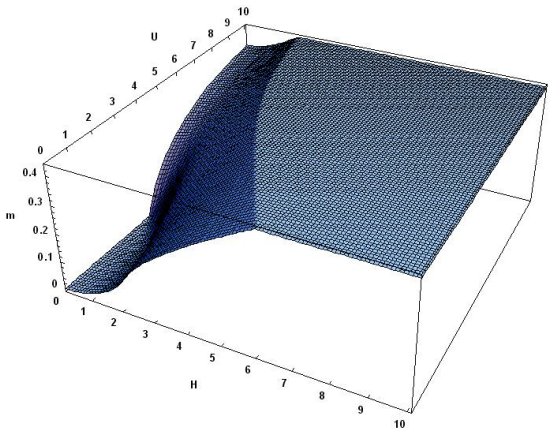


**Figure 2.4:** Total magnetization $m = \sqrt{m_x^2 + m_z^2}$.

appears in the spectrum (see section 2.5), while $m_z$ does not exist for $H = 0$ as expected. The increase of $m_x(H)$ with growing external field when $U < U_c$ can be traced to the nesting of the Fermi surface. The Fermi surface is point like for the free systems and has circular shape for $H > 0$ and $H = 0, U > U_c$. As already mentioned above nesting happens in our case at $\mathbf{Q}_{nest} = (0, 0)$ that is the nesting condition $\epsilon(\mathbf{k} + \mathbf{Q}_{nest}) = -\epsilon(\mathbf{k})$ is altered to

$$E_i(\mathbf{k}, \uparrow) = -E_j(\mathbf{k}, \downarrow) \; . \tag{2.37}$$

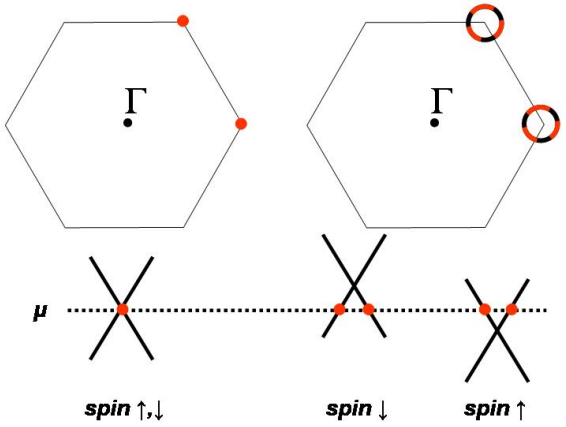


**Figure 2.5:** Visualization of the nesting of up and down spin Fermi surface. In case of $H = 0$ (free system, left) the up and down bands collapse onto each other, whereas for $H > 0$ the bands are shifted by virtue of the magnetic field (right).

Thus, nesting connects the up-spin Fermi line with the down-spin Fermi line. Without a magnetic field, in the honeycomb lattice nesting is intrinsically extremely weak compared to the perfect nesting in the square lattice [17]. The picture is consistent with the logarithmic divergence of $\chi_{AFM}(T)$. This leads to a spin-density wave with alternating spins in the two orbitals at low magnetic fields. The behaviour of $m_x$ is governed by two competing processes each of which seeks to minimize the free energy of the system. The magnetic field tries to align the spins and therefore avoids canted electron spins. On the other side canted antiferromagnetism opens up a energy gap in the spectrum and thereby lowers the energy. When the external field is big enough the lattice is totally polarized that is transversal magnetization disappears for the benefit of vertical magnetization.

## 2.5 Spectral function

All information about the single particle excitations like the one particle density of states can be derived from the one particle Green function and the spectral density. The Green function $G_{x,y}(t_1, t_2)$ is the amplitude for the propagation of an electron or a one particle

excitation from a state, characterized by the quantum number $x$ and time $t_1$ to the state $y$ at time $t_2$. Thermal (imaginary time) and zero temperature (real time) Green functions may be transformed into each other by considering a more general Green function in the complex $t_1 - t_2$ plane. The physical relevant entities, which depend on real time and frequency, may be obtained upon analytic continuation [1]. The Matsubara Green function in imaginary time is defined as (with the time ordering operator $T_\tau$)

$$G_{x,y}(\tau_1,\tau_2) = -\langle T_\tau[\hat{c}_x(\tau_1)\hat{c}_y^\dagger(\tau_2)]\rangle = \langle \hat{c}_x(\tau_1)\hat{c}_y^\dagger(\tau_2)\rangle \;\; for\; \tau_1 > \tau_2 \; . \tag{2.38}$$

With (2.30) and (2.31)the one particle Green function reads

$$\begin{aligned} G_{m,n}(\tau) &= -\langle \hat{c}_m(\tau)\hat{c}_n^\dagger(0)\rangle \\ &= -\sum_{m\prime,n\prime} \mathbf{U}^\dagger_{m,m\prime}\mathbf{U}_{n\prime,n}\langle \hat{\gamma}_{m\prime}(\tau)\hat{\gamma}^\dagger_{n\prime}(0)\rangle \\ &= -\sum_{m\prime,n\prime} \mathbf{U}^\dagger_{m,m\prime}\mathbf{U}_{n\prime,n}\langle \hat{\gamma}_{m\prime}(\tau)\hat{\gamma}^\dagger_{n\prime}(0)\rangle\delta_{m\prime,n\prime} \\ &= -\sum_{m\prime} \mathbf{U}^\dagger_{m,m\prime}\mathbf{U}_{m\prime,n}\langle \hat{\gamma}_{m\prime}(\tau)\hat{\gamma}^\dagger_{m\prime}(0)\rangle \; . \end{aligned} \tag{2.39}$$

The frequency dependent Matsubara Green function is

$$\begin{aligned} G_{m,n}(\omega_s) &= \int_0^\beta d\tau G(\tau)e^{\imath\omega_s\tau} \\ &= -\int_0^\beta d\tau \sum_{m\prime} \mathbf{U}^\dagger_{m,m\prime}\mathbf{U}_{m\prime,n}\langle \hat{\gamma}_{m\prime}(\tau)\hat{\gamma}^\dagger_{m\prime}(0)\rangle e^{\imath\omega_s\tau} \\ &= -\int_0^\beta d\tau \sum_{m\prime} \mathbf{U}^\dagger_{m,m\prime}\mathbf{U}_{m\prime,n}\langle \hat{\gamma}_{m\prime}\hat{\gamma}^\dagger_{m\prime}\rangle e^{(\imath\omega_s - E_{m\prime})\tau} \\ &= -\sum_{m\prime} \mathbf{U}^\dagger_{m,m\prime}\mathbf{U}_{m\prime,n}\langle \hat{\gamma}_{m\prime}\hat{\gamma}^\dagger_{m\prime}\rangle \frac{e^{(\imath\omega_s - E_{m\prime})\beta} - 1}{\imath\omega_s - E_{m\prime}} \\ &= -\sum_{m\prime} \mathbf{U}^\dagger_{m,m\prime}\mathbf{U}_{m\prime,n}\frac{e^{\beta E_{m\prime}}}{e^{\beta E_{m\prime}} + 1}\frac{e^{(\imath\omega_s - E_{m\prime})\beta} - 1}{\imath\omega_s - E_{m\prime}} \\ &= -\sum_{m\prime} \mathbf{U}^\dagger_{m,m\prime}\mathbf{U}_{m\prime,n}\frac{e^{\imath\omega_s\beta} - e^{\beta E_{m\prime}}}{(e^{\beta E_{m\prime}} + 1)(\imath\omega_s - E_{m\prime})} \\ &= \sum_{m\prime} \mathbf{U}^\dagger_{m,m\prime}\mathbf{U}_{m\prime,n}\frac{1}{\imath\omega_s - E_{m\prime}} \; . \end{aligned} \tag{2.40}$$

To go from line six to line seven, $\omega_s = \frac{(2s+)\pi}{\beta}$ for Fermions was used.
In a many particle system the spectral function $A(\mathbf{k},\omega)$ describes the energy resolution of a particle in a given quantum state $\mathbf{k}$ or complementary at a given energy the resolution of the quantum state. To put it more distinctly, we inject in a $N$-particle system one additional (quasi-)particle with quantum number $\mathbf{k}$ and can read from the shape of the spectral function at $\mathbf{k}$ the lifetime of this excitation. Free particles have an infinite lifetime,

that is the spectral function has the form $A(\mathbf{k},\omega) \propto \delta(w - E(\mathbf{k}))$ with the eigenvalues $E(\mathbf{k})$ of the free Hamiltonian. In the case of non-interacting electrons an excitation of energy $\omega$ can be only created in the state $\mathbf{k}$ with energy $E(\mathbf{k}) = \omega$. Interactions like electron-electrons interactions or electron-phonon interactions broaden the spectral profile and cause a redistribution of spectral weight. The mean field Hamiltonian was solved by introducing quasiparticle operators, that is the hybridization of $\hat{c}_{\uparrow,\downarrow}$- und $\hat{d}_{\uparrow,\downarrow}$-electrons which enter the quasiparticle with a $\mathbf{k}$-dependent weight. This allows us to write down the single particle spectral function. The spectral function is defined via the imaginary part of the analytic continuation of the Matsubara Green function:

$$A_{m,n}(\mathbf{k},\omega) = -\frac{1}{\pi} Im\, G_{m,n}(\omega_s \to \omega + \imath 0^+) \tag{2.41}$$

with

$$G_{m,n}(\omega) = \sum_{m\prime} \mathbf{U}^{\dagger}_{m,m\prime}\mathbf{U}_{m\prime,n} \frac{1}{\omega - E_{m\prime} + \imath 0^+} \ . \tag{2.42}$$

Using the Dirac identity $Im\frac{1}{x-x_0+\imath 0^+} = -\pi\delta(x - x_0)$ it follows that

$$A_{m,n}(\mathbf{k},\omega) = \sum_{m\prime} \mathbf{U}^{\dagger}_{m,m\prime}\mathbf{U}_{m\prime,n}\delta(\omega - E_{m\prime}) \ . \tag{2.43}$$

The poles of the Green function thus enter the spectral function with a spectral weight. By virtue of the unitarity of $\mathbf{U}$ we have

$$\sum_{m\prime} \mathbf{U}^{\dagger}_{m,m\prime}\mathbf{U}_{m\prime,n} = \mathbf{1} \ , \tag{2.44}$$

and therefore

$$\int_{-\infty}^{+\infty} d\omega A(\mathbf{k},\omega) = 1 \quad . \tag{2.45}$$

Hence the spectral weight is conserved. Given the spectral function in the first Brillouin zone, the one particle density of states follows as

$$\rho(\omega) = \frac{1}{N}\sum_{\mathbf{k}} A(\mathbf{k},\omega) \ . \tag{2.46}$$

To plot the spectral function as a function of $\mathbf{k}$ and $\omega$ with its corresponding weight, the delta distributions were numerically implemented as Lorentz curves with small but finite width $\Delta_L$. $A_{\downarrow,\downarrow}(\mathbf{k},\omega)$ and the concomitant density of states is shown for the different phases of the mean field ansatz (Fig.2.5, Fig.2.5). The evolution of the Fermi surface is plotted in Fig(2.6).

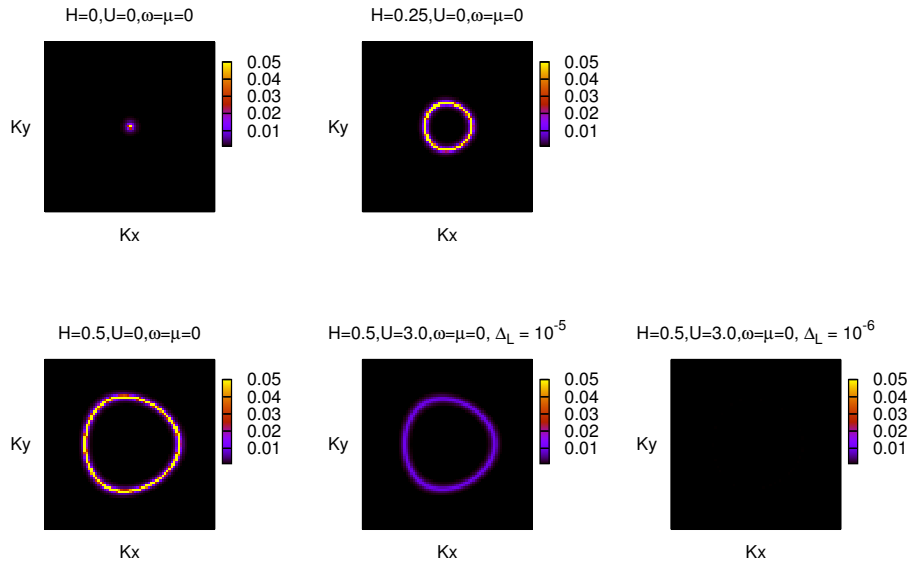


**Figure 2.6:** Evolution of the Fermi surface around the Dirac point $K_x, K_y$. The Fermi point in case of the free systems acquires circular shape when the bands are shifted due to the field. As soon as the interaction is turned on (here $H = 0.5$, $U = 3$) the Fermi line vanishes in agreement with the opening of the gap. This is observed when the artificially introduced parameter for the width of the Lorentzian $\Delta_L$ is made small enough (bottom right).

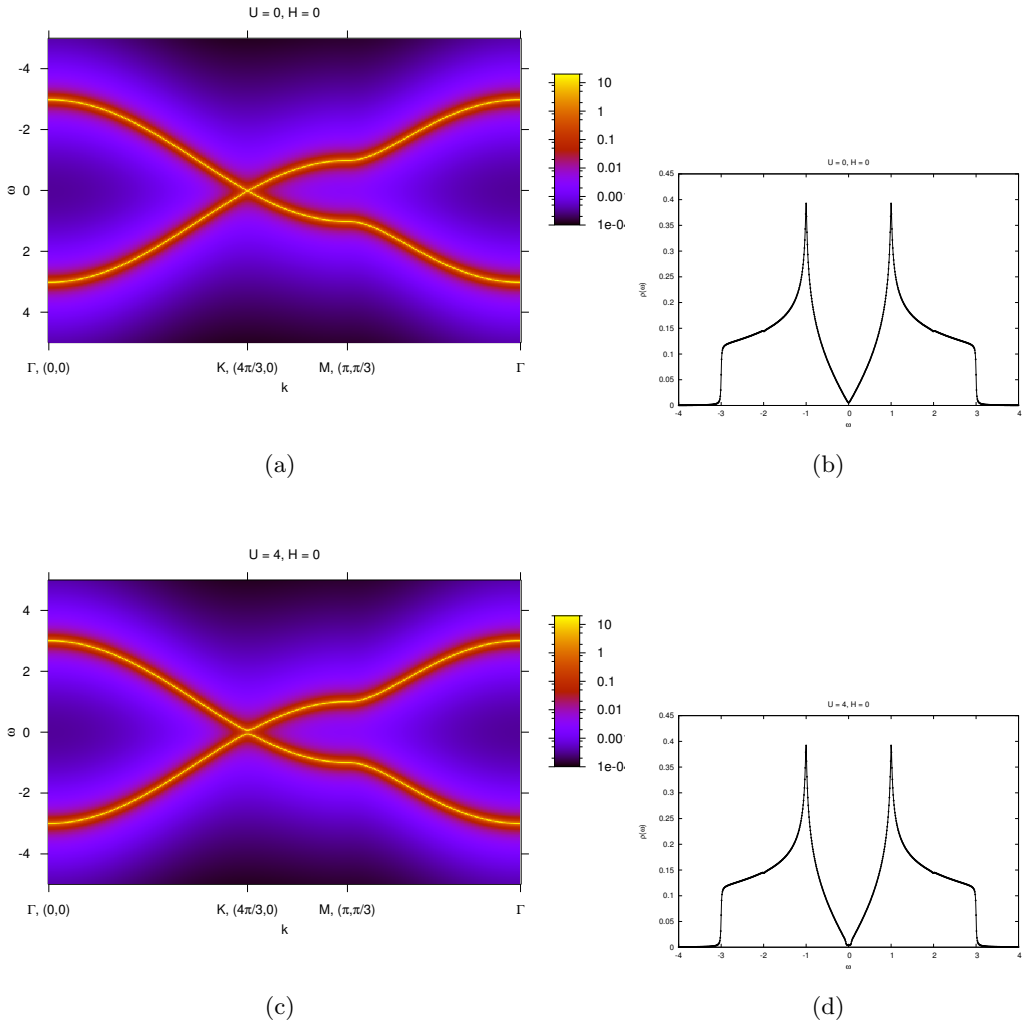


**Figure 2.7:** Single particle spectral function $A_{\downarrow,\downarrow}(\mathbf{k}, \omega)$ along the path of high symmetry $\Gamma$-$K$-$M$-$\Gamma$ of the first Brillouin zone and the concomitant density of states, for $H = 0$. The density of states can be linearized in the low energy limit around the Dirac points. The peaks signal van Hove singularities which occur as the slope of $E(\mathbf{k})$ goes to zero. In case of $U = U_c \approx 4$, the gap opens up.

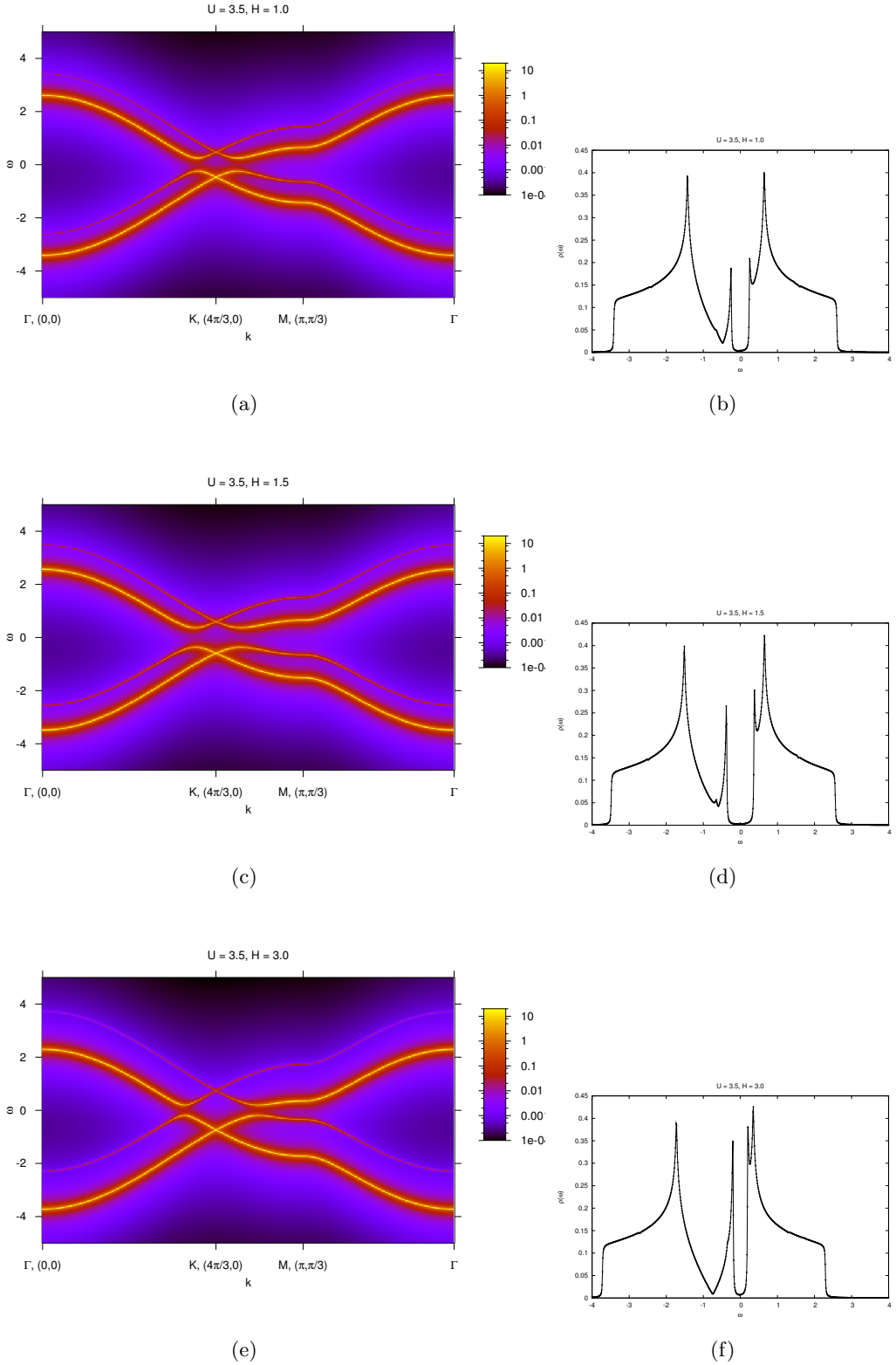


**Figure 2.8:** Single particle spectral function $A_{\downarrow,\downarrow}(\mathbf{k},\omega)$ and (spin down) density of states, at $U = 3.5$ fixed. From top to bottom we pass through the maximum of the gap (the transversal magnetization $m_x$) which occurs around $H = 1.5$. For $H > 1.5$ the gap gets smaller again as total polarization begins to set in.

# 3 Functional Integral Formulation

The formulation of the partition function as a functional integral is the starting point of the mathematical treatment of auxilliary field methods. In the present chapter it will be argued how the partition function may be rewritten as an integral over all possible configurations of a new variable, the auxilliary field.
The electron-electron interaction enters the Hamilton operator as a term with four fermionic creation and annihilation operators, that is the term is of quartic order in the operators. Introducing a field variable serves to reduce the interaction term to bilinear form, as it is already the case with the kinetic electron-hopping term. In the framework of this formulation the original electron-electron interaction is restated as an interaction of one-body operators with a (bosonic as it will turn out) external field. This mathematical transformation is accomplished with a Hubbard-Stratonovich decomposition.
Writing the partition function in a path integral representation is s fundamental concept of many quantum Monte Carlo (QMC) methods. This allows to map a $d$-dimensional quantum system to a $d+1$-dimensional classical system. The additional dimension is called imaginary time in analogy to the time evolution in quantum mechanics. The reason to discretize a time or temperature interval in infinitesimal steps lies in the general anticommunitativity of the summands in the Hamilton operator. Each subinterval may be calculated neglecting this decisive property of quantum mechanics. However, the resulting systematic error vanishes in the infinitesimal limit and can also be controlled at finite step width, as it is the case in the numerical simulation.

## 3.1 The partition function as a path integral over imaginary time

The path-integral representation of quantum mechanics can readily be applied to many particle systems as opposed to the standard formulation of quantum mechanics in terms of wave functions and the Schrödinger equation. In the Schrödinger picture of quantum mechanics, the amplitude for a particle to go from the coordinates $(x_i, t_i)$ to $(x_f, t_f)$ is given by the time evolution operator $U(t_f, t_i) = e^{-iH(t_f - t_i)}$ and its matrix elements $\langle x_f | e^{-iH(t_f - t_i)} | x_i \rangle$. In the path integral picture we want to reformulate the time evolution operator by evoking the superposition principle of quantum mechanics: in principle the transition $x_i \to x_f$ can be realized with every function or path $x(t)$ that begins at $x_i$ and ends at $x_f$. Each path gives one possible transition amplitude which may be written in

terms of a phase and the total amplitude is the coherent superposition of all contributions [8]:

$$\langle x_f|e^{-\frac{i}{\hbar}H(t_f-t_i)}|x_i\rangle = \sum_{path} e^{\frac{i}{\hbar}\cdot phase(path)} = \int D[x(t)]e^{\frac{i}{\hbar}\cdot phase} = \int_{x_i,t_i}^{x_f,t_f} D[x(t)]e^{\frac{i}{\hbar}S[x(t)]} \quad (3.1)$$

In the last step the Lagrangian action $S = \int Ldt$ was introduced. Identifying the phase with the action $S[x(t)]$ can be easily understood via the stationary phase approximation in the classical limit: the classical path should be stationary and fulfills the principle of least action [8].
The analogy between the Schrödinger time evolution operator and the density operator $e^{-\beta H}$ of statistical mechanics allows for the development of a path integral representation of the partition function $Z$. The partition function of the canonical ensemble is

$$Z = Tr\ e^{-\beta H} = \int dx \langle x|e^{-\beta H}|x\rangle\ . \quad (3.2)$$

and can be interpreted as the integral over the diagonal components of the evolution operator $U(\tau_f, \tau_i) = e^{-(\tau_f-\tau_i)H}$ which operates in imaginary or Euclidean time $\tau$. To evaluate (3.2) for a Hamiltonian with multiple summands, $H = \sum_i H_i$ we make use of the Trotter formula [36]

$$e^{-\beta H} = \lim_{m\to\infty} \prod_{l=1}^{m} \Big( \prod_i e^{-\Delta\tau H_i} \Big) \quad (3.3)$$

with $m\Delta\tau = \beta$ and $\prod_i e^{-\Delta\tau H_i} = e^{-\Delta\tau H} + O(\Delta\tau^2)$. What we gain is twofold: first,we splitted the evolution from $0 \to \beta$ in $m$ small pieces of length $\Delta\tau$, the time slices. Chained together the matrix elements of all time slices give the total matrix element. Secondly, on each time slice we are able to compute the corresponding matrix element since the exponentiated Hamiltonian is simplified in terms of a product of exponentials. The price we pay is an error of the order $\Delta\tau^2$ when we are not able to let $m$ go to infinity or $\Delta\tau$ to zero, respectively. The partition function is therefore

$$\begin{aligned} Z_{exact} &= \int dx\ U(\tau_i, \tau_f)|_{x_i=x_f=x;\ \tau_i=0,\tau_f=\beta} \\ &= \int dx \Big( \lim_{m\to\infty} \langle x_f|(e^{-\Delta\tau H})^m|x_i\rangle \Big) |_{x_i=x_f=x;\ \tau_i=0,\tau_f=\beta} \\ &= \int dx \lim_{m\to\infty} \langle x_f| \Big( \prod_i e^{-\Delta\tau H_i} \Big)^m |x_i\rangle|_{x_i=x_f=x;\ \tau_i=0,\tau_f=\beta} \\ &= \int dx \int_{x_i=x,\tau_i=0}^{x_f=x,\tau_f=\beta} D[x(\tau)]e^{-\widetilde{S}[x(\tau)]}\ . \end{aligned} \quad (3.4)$$

In the last line the Euclidean action $\widetilde{S}[x(t)]$ was introduced [7]. Using this so-called first order Trotter decomposition (3.3), it has been shown in case of large but finite $m$ that

for the partition function and the expectation value of Hermitian operators the correction term linear in $\Delta\tau$ vanishes. As pointed out in [36] this is true if all relevant operators are simultaneously real representable.
In practice we have to deal with a Hamiltonian with two contributions, $H = H_T + H_I$. The partition function to evaluate, respectively to sample with Monte-Carlo methods is then

$$Z = Tr[e^{-\beta H}] = Tr\Big[\Big(e^{-\Delta\tau H_I} e^{-\Delta\tau H_T}\Big)^m\Big] + \mathcal{O}(\Delta\tau^2)\ . \tag{3.5}$$

From now on we understand the partition function to be correct except for an error of the order $\mathcal{O}(\Delta\tau^2)$ and omit the discretization error in the notation.

## 3.2 Introduction of the auxiliary field

To evaluate the potential part of the partition function which was isolated by means of the Trotter decomposition on every single time slice the two-body term has to be rewritten in one-body notation. This is possible by introducing an auxiliary variable $s_i$ called the auxiliary field. We consider the generic Hamilton operator of a fermionic system,

$$H = H_T + H_I = \sum_{i,j} c_i^\dagger T_{i,j} c_j + \frac{1}{2}\sum_{i,j,k,l} V_{i,j,k,l} c_i^\dagger c_k c_j^\dagger c_l\ . \tag{3.6}$$

The matrices $T$ and $V$ are generalized hopping and interaction matrices. In many cases the restriction is hopping processes to nearest neighbours only, spin conservation and to the on-site interaction. Applying the Trotter decomposition the operator on one single time slice is

$$\begin{aligned} \lim_{\Delta\tau\to 0} e^{-\Delta\tau H} &= \lim_{\Delta\tau\to 0}\Big(e^{-\Delta\tau H_I} e^{-\Delta\tau H_T}\Big) \\ &= \lim_{\Delta\tau\to 0}\Big(\underbrace{e^{-\frac{\Delta\tau}{2}\sum_{i,j,k,l} V_{i,j,k,l} c_i^\dagger c_k c_j^\dagger c_l}}_{\text{two-body operator}}\ e^{-\Delta\tau\sum_{i,j} c_i^\dagger T_{i,j} c_j}\Big)\ . \end{aligned} \tag{3.7}$$

Now we concentrate on the two-body operator which may be rewritten using a Hubbard-Stratonovich (HS) transformation. Generally spoken, this transformation allows for the mapping of an interacting fermion problem to a system of non interacting fermions coupled to a fluctuating external field [37]. The HS transformation is based on the identity for multidimensional integral over the real variables $\mathbf{A}_{i,j}, \mathbf{J}_i, s_i$

$$e^{\frac{1}{2}\sum_{i,j}\mathbf{J}_i\mathbf{A}_{i,j}\mathbf{J}_j} = \sqrt{det[\mathbf{A}^{-1}]}\int ds(i) e^{-\frac{1}{2}s_i\mathbf{A}^{-1}_{i,j}s_j + s_i\mathbf{J}_i}\ , \tag{3.8}$$

with the measure $ds(i) = \prod_i \frac{ds_i}{\sqrt{2\pi}}$.[1] This identity is an extension of the familiar Gaussian integral formula [1]. We are allowed to interprete (3.8) as operator identity, using the one

[1] The matrix $\mathbf{A}$ is assumed to be real, symmetric and positive definite.

body operators $(c^\dagger c)_m, (c^\dagger c)_n$. Here a short notation for the indices, $m \equiv (i,k), n \equiv (j,l)$, is introduced. The interaction term then reads

$$\begin{aligned} & e^{-\frac{\Delta\tau}{2}\sum_{m,n}(c^\dagger c)_m V_{m,n}(c^\dagger c)_n} \\ = \quad & \sqrt{det[\Delta\tau(V_{m,n})^{-1}]}\int ds(m)\; e^{\frac{\Delta\tau}{2}\sum_{m,n} s_m(V_{m,n})^{-1}s_n - \Delta\tau\sum_m s_m(c^\dagger c)_m}\;. \end{aligned} \tag{3.9}$$

We succeeded in writing the interaction part of the imaginary time evolution operators as an integral over one-body operators. This is done at the expense of a new variable, the auxilliary field $s(i)$. Since the HS-transformation is applied independently on every time slice, the auxilliary field is a function of lattice site and time slice index, $s = s(i,\tau)$.

## 3.3 Discrete Hubbard-Stratonovich transformation

The HS is not singular and the efficiency of an algorithm relies to great degree on the chosen transformation. In principle the partition function based on (3.9) may be calculated with Monte Carlo methods. However it is more efficient to carry out a summation over discrete field values than to integrate over a continuous field since the phase space over which the integral has to be performed is much smaller in the former formulation than it is in the Gaussian one [37]. The notation in this section and in the following section is based on [5]. Initially we consider the Hubbard interaction

$$H_I = U(c_\uparrow^\dagger c_\uparrow - \frac{1}{2})(c_\downarrow^\dagger c_\downarrow - \frac{1}{2}) = -\frac{U}{2}(n_\uparrow - n_\downarrow)^2 + \frac{U}{4} \tag{3.10}$$

for a single lattice site and time slice and construct the general case of $N$ sites and $\beta/\Delta\tau$ time slices later. The Hilbert space on a single site is four dimensional, $\mathcal{H} = \mathcal{H}^0 \otimes \mathcal{H}^1 \otimes \mathcal{H}^2$, and is spanned by the four states, $\mathcal{H} = \{|0\rangle, |\uparrow\rangle, |\downarrow\rangle, |\uparrow\downarrow\rangle\}$. Therefore

$$e^{-\Delta\tau H_I} = \gamma \sum_{s=\pm 1} e^{\alpha s(n_\uparrow - n_\downarrow)} \tag{3.11}$$

may be a possible HS transformation over the field $s$ with values $\pm 1$ if we succeed in finding compatible values for $\alpha$ and $\gamma$. Applying the state kets $|0\rangle$,$|\uparrow\rangle$,$|\downarrow\rangle$,$|\uparrow\downarrow\rangle$ on (3.11) one ends up with the following equations

$$\begin{aligned} e^{-\Delta\tau H_I}|0\rangle &= e^{-\frac{\Delta\tau U}{4}}|0\rangle = 2\gamma|0\rangle \\ e^{-\Delta\tau H_I}|\uparrow\rangle &= e^{+\frac{\Delta\tau U}{4}}|\uparrow\rangle = \gamma(e^\alpha + e^{-\alpha})|\uparrow\rangle = 2\gamma cosh(\alpha)|\uparrow\rangle \\ e^{-\Delta\tau H_I}|\downarrow\rangle &= e^{+\frac{\Delta\tau U}{4}}|\downarrow\rangle = \gamma(e^\alpha + e^{-\alpha})|\downarrow\rangle = 2\gamma cosh(\alpha)|\downarrow\rangle \\ e^{-\Delta\tau H_I}|\uparrow\downarrow\rangle &= e^{-\frac{\Delta\tau U}{4}}|\uparrow\downarrow\rangle = 2\gamma|\uparrow\downarrow\rangle \end{aligned} \tag{3.12}$$

That is, the discrete HS transformation (3.11) is valid provided that $\gamma$ and $\alpha$ take the values

$$\gamma = \frac{e^{-\frac{\Delta\tau U}{4}}}{2}, \quad cosh(\alpha) = e^{\frac{\Delta\tau U}{2}}. \tag{3.13}$$

Since the HS variable $s$ couples to the $z$-component of the magnetization $m_z = (n_\uparrow - n_\downarrow)$ the $SU(2)$ spin symmetry is broken for each field and is only reestablished after summing over all fields. This symmetry breaking may be circumvented using complex HS transformations which couple to the electron density. This is discussed in [5].
The expression (3.11) can easily generalized to a $N$-particle system which is in our case a lattice with $N$ sites:

$$e^{-\Delta\tau U \sum_i (n_{i,\uparrow}-\frac{1}{2})(n_{i,\downarrow}-\frac{1}{2})} = C \sum_{s_1,s_2,\cdots,s_N=\pm 1} e^{\alpha \sum_i s_i (n_{i,\uparrow}-n_{i,\downarrow})} , \tag{3.14}$$

with $C = \frac{e^{\frac{-\Delta\tau U N}{4}}}{2^N}$. To conclude, the on-site interaction may be replaced by a fluctuating field composed of Ising variables $s_i = \pm$ which couples to the magnetic field.

## 3.4 Formulation of the partition function

Summarizing the preceding three sections we have established the necessary mathematics to write down the partition function as it is needed for the Monte Carlo method. Before proceeding we introduce a simplified vector notation. The hopping term is

$$H_T = -t \sum_{\langle i,j\rangle,\sigma} c^\dagger_{i,\sigma} c_{j,\sigma} = -t \sum_{\langle i,j\rangle,\sigma,\sigma\prime} c^\dagger_{i,\sigma} c_{j,\sigma\prime} \delta_{\sigma,\sigma\prime} = \sum_{x,y} c^\dagger_x T_{x,y} c_y \equiv \mathbf{c}^\dagger \mathbf{T} \mathbf{c} , \tag{3.15}$$

with $x = (i,\sigma)$. The HS transformation of the interaction can be written similarly as

$$\begin{aligned} \alpha \sum_i s_i (n_{i,\uparrow} - n_{i,\downarrow}) &= \alpha \sum_{i,\sigma} s_i p_\sigma c^\dagger_{i,\sigma} c_{i,\sigma} \\ &= \sum_{i,\sigma,i\prime,\sigma\prime} \alpha s_i p_\sigma \delta_{i,i\prime} \delta_{\sigma,\sigma\prime} c^\dagger_{i,\sigma} c_{i\prime,\sigma\prime} = \sum_{x,y} c^\dagger_x V(\mathbf{s})_{x,y} c_y \equiv \mathbf{c}^\dagger \mathbf{V} \mathbf{c} . \end{aligned} \tag{3.16}$$

Now we interpret the Ising field on time slice $n$ as a $N$-dimensional vector $\mathbf{s}_n$ the elements of which take the values $\pm 1$. Finally the grand canonical partition function reads

$$\begin{aligned}
Z &= Tr\left[e^{-\beta\left(H-\mu N\right)}\right] \\
&= Tr\left[\left(e^{-\Delta\tau H_I}e^{-\Delta\tau H_T}\right)^m\right] + O(\Delta\tau^2) \\
&= Tr\left[\left(C\sum_{s_1,s_2,\cdots,s_N=\pm 1} e^{\alpha\sum_i s_i(n_{i,\uparrow}-n_{i,\downarrow})}e^{-\Delta\tau(-t\sum_{\langle i,j\rangle,\sigma}c^\dagger_{i,\sigma}c_{j,\sigma})}\right)^m\right] \\
&= C^m\, Tr\left[\prod_{n=1}^{m}\sum_{\mathbf{s}_n} e^{\mathbf{c}^\dagger\mathbf{V}(\mathbf{s}_n)\mathbf{c}}e^{-\Delta\tau\mathbf{c}^\dagger\mathbf{T}\mathbf{c}}\right] \\
&= C^m \sum_{\mathbf{s}_1,\mathbf{s}_2,\cdots,\mathbf{s}_n} Tr\underbrace{\left[\prod_{n=1}^{m} e^{\mathbf{c}^\dagger\mathbf{V}(\mathbf{s}_n)\mathbf{c}}e^{-\Delta\tau\mathbf{c}^\dagger\mathbf{T}\mathbf{c}}\right]}_{U_{\mathbf{s}}(\beta,0)} \\
&= C^m \sum_{\mathbf{s}_1,\mathbf{s}_2,\cdots,\mathbf{s}_m} Tr\left[U_{\mathbf{s}}(\beta,0)\right] \qquad (3.17)
\end{aligned}$$

In line two, the chemical potential can be absorbed in a redefinition of $H_T$. The partition function now is the trace over a the sum of propagators $U_s(\beta,0)$ in imaginary time. Using the following relation[2] for the bilinear operators $\mathbf{c}^\dagger A_1\mathbf{c},\cdots,\mathbf{c}^\dagger A_n\mathbf{c}$,

$$Tr[e^{\mathbf{c}^\dagger\mathbf{A}_1\mathbf{c}}e^{\mathbf{c}^\dagger\mathbf{A}_2\mathbf{c}}\cdots e^{\mathbf{c}^\dagger\mathbf{A}_n\mathbf{c}}] = det[\mathbf{1}+e^{\mathbf{A}_1}e^{\mathbf{A}_2}\cdots e^{\mathbf{A}_n}]\,, \qquad (3.18)$$

the trace (3.17) can be evaluated explicitly by writing it as determinant of matrices. This technique is known as integrating out the fermionic degrees of freedom. With the matrix representation of the propagator,

$$B_{\mathbf{s}}(\beta,0) = \prod_{n=1}^{m} e^{\mathbf{V}(\mathbf{s}_n)}e^{-\Delta\tau\mathbf{T}}\,, \qquad (3.19)$$

the final version of (3.17) is (with $m\Delta\tau=\beta$)

$$Z = C^m \sum_{\mathbf{s}_1,\mathbf{s}_2,\cdots,\mathbf{s}_m} det[\mathbf{1}+B_{\mathbf{s}}(\beta,0)]\,. \qquad (3.20)$$

This is the general finite temperature result which is the basis of the finite temperature QMC (FTQMC) algorithm. This method relies on the grand canonical ensemble. However if one is soley interested in ground state results it is more efficient to use a canonical approach which is subject of Chapter 4.

[2] A detailed proof may be found in [5]

# 4 The Projector QMC Method

Within the framework of auxilliary field quantum Monte Carlo methods, simulations can be realized for finite temperatures or at zero temperature. In the latter case, the algorithm approximates the (unknown) ground state wave function $\Psi_0$ by repeatedly projecting of a trial wave function $\Psi_T$ and therefore is called projector quantum Monte Carlo (PQMC) algorithm. The trial wave function is chosen to be a Slater determinant.
In this chapter the basic principles of the PQMC algorithm are explained. The essential building block is the equal time Green function, which determines the Monte Carlo sampling and also makes possible the calculation of arbitrary static observables via Wick's theorem. Subsequently, it will be shown how both equal time and imaginary time displaced Green functions can be implemented into the algorithm to give reliable and numerically stable results.

## 4.1 The trial wave function

As it has been shown in the preceding chapter the partition function and thus the expectation values may be obtained based on the knowledge of all field variables. To reduce complexity one will later on only use the most probable configurations of field variables. This is accomplished by the actual Monte Carlo part of the algorithm (see chapter 5).
In the following we argue that the trial wave function $|\Psi_T\rangle$ can be written as a product of one particle states. We adopt the notation of [5]. In anticipation of a future result (4.9) one has

$$\frac{\langle\Psi_0|A|\Psi_0\rangle}{\langle\Psi_0|\Psi_0\rangle} = \lim_{\theta\to\infty} \frac{\langle\Psi_T|e^{-\theta H}Ae^{-\theta H}|\Psi_T\rangle}{\langle\Psi_T|e^{-2\theta H}|\Psi_T\rangle} = \lim_{\theta\to\infty} \sum_{\mathbf{s}} P_{\mathbf{s}} A_{\mathbf{s}} + O(\Delta\tau^2) \tag{4.1}$$

Thus the expectation value of $A$ is given by the sum over all HS-fields with a suitable normalized weight $P_{\mathbf{s}}$. The second equation in (4.1) is obtained by assuming a non degenerate ground state $|\Psi_0\rangle$, with $\langle\Psi_T|\Psi_0\rangle \neq 0$ and $H|n\rangle = E_n|n\rangle$:

$$\begin{aligned}
\lim_{\theta\to\infty} \frac{\langle\Psi_T|e^{-\theta H}Ae^{-\theta H}|\Psi_T\rangle}{\langle\Psi_T|e^{-2\theta H}|\Psi_T\rangle} &= \lim_{\theta\to\infty} \frac{\sum_{n,m}\langle\Psi_T|n\rangle\langle n|e^{-\theta H}Ae^{-\theta H}|m\rangle\langle m|\Psi_T\rangle}{\sum_n \langle\Psi_T|e^{-2\theta H}|n\rangle\langle n|\Psi_T\rangle} \\
&= \lim_{\theta\to\infty} \frac{\sum_{n,m}\langle\Psi_T|n\rangle\langle m|\Psi_T\rangle\langle n|A|m\rangle e^{-\theta(E_n+E_m)}}{\sum_n |\langle\Psi_T|n\rangle|^2 e^{-2\theta E_n}} \\
&= \frac{\langle\Psi_0|A|\Psi_0\rangle}{\langle\Psi_0|\Psi_0\rangle}
\end{aligned} \tag{4.2}$$

If one inserts the HS-formulation of the Hamilton operator, (4.2) describes the propagation (in imaginary time) of a trial wave function $|\Psi_T\rangle$ in a system of non-interacting fermions under the influence of an external field. The total wave function of non interacting particles can be formed with single particle wave functions.
The many body state of $N_P$ particles which can occupy $N_S$ single particle states ($N_P \leq N_S$) is given by a Slater determinant. The following notation is adopted from [5]. We consider the one-particle Hamiltonian $H_0$ which is diagonalized by virtue of the unitarian transformation $U$, $U^\dagger h U = diag(\lambda_1 \cdots \lambda_{N_S})$.

$$H_0 = \sum_{x,y}^{N_S} c_x^\dagger h_{x,y} c_y = \sum_{x,y}^{N_S} c_x^\dagger U U^\dagger h_{x,y} U U^\dagger c_y = \sum_{x}^{N_S} \lambda_{x,x} \gamma_x^\dagger \gamma_x \ . \tag{4.3}$$

A many body state $|\Psi\rangle$ with $N_P$-particle occupying the single particle states $\alpha_1 \cdots \alpha_{N_P}$ is therefore written as

$$|\Psi\rangle = \prod_{n=1}^{N_P} \gamma_{\alpha_n}^\dagger |0\rangle = \prod_{n=1}^{N_P} \left( \sum_x c_x^\dagger U_{x,\alpha_n} \right) |0\rangle = \prod_{n=1}^{N_P} \left( \mathbf{c}^\dagger \mathbf{P} \right)_n |0\rangle \ . \tag{4.4}$$

The $N_S$x$N_P$-matrix $\mathbf{P}$ thus completely determines the many body state. The Slater determinant stays a Slater determinant under propagation with a one particle propagator,

$$e^{\mathbf{c}^\dagger \mathbf{T} \mathbf{c}} \prod_{n=1}^{N_P} \left( \mathbf{c}^\dagger \mathbf{P} \right)_n |0\rangle = \prod_{n=1}^{N_P} \left( \mathbf{c}^\dagger e^{\mathbf{T}} \mathbf{P} \right)_n |0\rangle \ . \tag{4.5}$$

This is true in the case of $\mathbf{T}$ (anti-)hermitian. Furthermore the overlap of two Slater determinants $|\Psi\rangle$ and $|\tilde{\Psi}\rangle$ evaluates to

$$\langle \Psi | \tilde{\Psi} \rangle = det[\mathbf{P}^\dagger \tilde{\mathbf{P}}] \ . \tag{4.6}$$

A detailed proof of the above statements is presented in [5].
To sum up, in the PQMC algorithm the matrix $\mathbf{P}$ which determines the trial wave function is propagated:

$$|\Psi_T\rangle = \prod_{n=1}^{N_P} \left( \mathbf{c}^\dagger \mathbf{P} \right)_n |0\rangle \ . \tag{4.7}$$

The scalar product of $|\Psi_T\rangle$ and the propagated wave function $e^{-2\theta H}|\Psi_T\rangle$ can be expressed as a sum over HS fields with the definition of the overlap of two Slater determinants (4.6) and the propagator $B(2\theta, 0)$ (3.19)

$$\langle \Psi_T | e^{-2\theta H} | \Psi_T \rangle = C^m \sum_{\mathbf{s}_1, \mathbf{s}_2, \cdots, \mathbf{s}_m} det[\mathbf{P}^\dagger B_{\mathbf{s}}(2\theta, 0) \mathbf{P}] \ . \tag{4.8}$$

The projection parameter or "temperature" $\theta$ and the disrete time-step $\Delta\tau$ define the number of trotter slices which are used for the propagation over the interval $[0, 2\theta]$. The limit to $\theta \to \infty$ may be reach upon extrapolation but converging behaviour is already observed for relatively small values of $\theta$ (Fig.4.1).

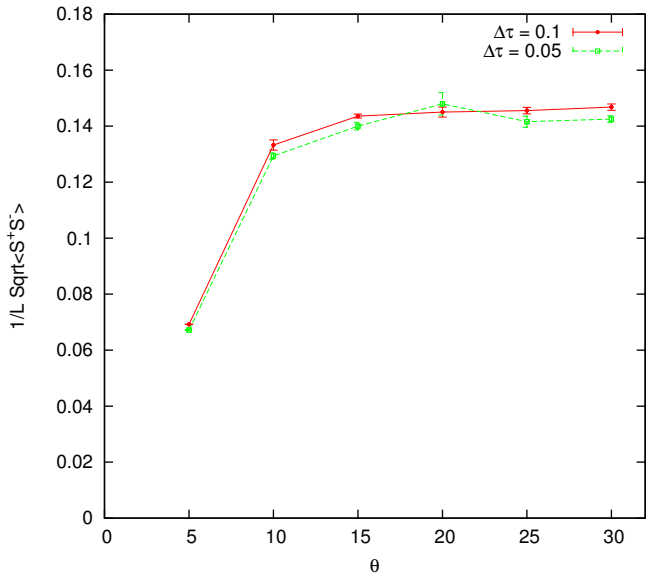


**Figure 4.1:** Convergence of PQMC Data for the transversal magnetization $\frac{1}{N}\sqrt{\langle S^+S^-\rangle}$ as a function of the projection parameter $\theta$ and temperature $\Delta\tau$ (lattice size $12 \times 12$, magnetization $m_z = 1/4$). For subsequent simulation the parameters $\theta = 20$ and $\Delta\tau = 0.1$ were used.

## 4.2 Observables in the PQMC algorithm

The expectation value of an observable for a given projection parameter $\theta$ is

$$\begin{aligned}
\frac{\langle\Psi_T|e^{-\theta H}Ae^{-\theta H}|\Psi_T\rangle}{\langle\Psi_T|e^{-2\theta H}|\Psi_T\rangle} &= \frac{\sum_{\mathbf{s}}\langle\Psi_T|U_{\mathbf{s}}(2\theta,\theta)AU_{\mathbf{s}}(\theta,0)|\Psi_T\rangle}{\sum_{\mathbf{s}}\langle\Psi_T|U_{\mathbf{s}}(2\theta,0)|\Psi_T\rangle} \\
&= \frac{\sum_{\mathbf{s}}\langle\Psi_T|U_{\mathbf{s}}(2\theta,\theta)AU_{\mathbf{s}}(\theta,0)|\Psi_T\rangle}{\sum_{\mathbf{s}}\langle\Psi_T|U_{\mathbf{s}}(2\theta,0)|\Psi_T\rangle}\ \frac{\langle\Psi_T|e^{-2\theta H}|\Psi_T\rangle}{\langle\Psi_T|e^{-2\theta H}|\Psi_T\rangle} \\
&= \frac{\sum_{\mathbf{s}}\langle\Psi_T|U_{\mathbf{s}}(2\theta,\theta)AU_{\mathbf{s}}(\theta,0)|\Psi_T\rangle}{\sum_{\mathbf{s}}\langle\Psi_T|U_{\mathbf{s}}(2\theta,0)|\Psi_T\rangle}\ \frac{det[\mathbf{P}^\dagger B_{\mathbf{s}}(2\theta,0)\mathbf{P}]}{\langle\Psi_T|U_{\mathbf{s}}(2\theta,0)|\Psi_T\rangle} \\
&= \frac{det[\mathbf{P}^\dagger B_{\mathbf{s}}(2\theta,0)\mathbf{P}]}{\sum_{\mathbf{s}}\langle\Psi_T|U_{\mathbf{s}}(2\theta,0)|\Psi_T\rangle}\ \frac{\sum_{\mathbf{s}}\langle\Psi_T|U_{\mathbf{s}}(2\theta,\theta)AU_{\mathbf{s}}(\theta,0)|\Psi_T\rangle}{\langle\Psi_T|U_{\mathbf{s}}(2\theta,0)|\Psi_T\rangle} \\
&= \sum_{\mathbf{s}} \underbrace{\frac{det[\mathbf{P}^\dagger B_{\mathbf{s}}(2\theta,0)\mathbf{P}]}{\sum_{\mathbf{s}}\langle\Psi_T|U_{\mathbf{s}}(2\theta,0)|\Psi_T\rangle}}_{P_{\mathbf{s}}}\ \underbrace{\frac{\langle\Psi_T|U_{\mathbf{s}}(2\theta,\theta)AU_{\mathbf{s}}(\theta,0)|\Psi_T\rangle}{\langle\Psi_T|U_{\mathbf{s}}(2\theta,0)|\Psi_T\rangle}}_{\langle A\rangle_{\mathbf{s}}} \\
&= \sum_{\mathbf{s}} P_{\mathbf{s}}\ \langle A\rangle_{\mathbf{s}}.
\end{aligned} \tag{4.9}$$

### 4.2.1 Equal time Green function $G(\tau)$

Based on the formulation with $\mathbf{P}$-matrices and the propagator $B_{\mathbf{s}}$ correlation functions can be calculated for a fixed field $\mathbf{s}$. Additionally one can demonstrate that every many-body Green function $\langle c^\dagger_{x_n} c_{y_n} \cdots c^\dagger_{x_2} c_{y_2} c^\dagger_{x_1} c_{y_1}\rangle$ can be split in a sum of one particle Green functions

$\langle c_x^\dagger c_y \rangle$. In other words, Wick's theorem is applicable. In the following the equal time Green function is calculated, the evaluation of multi-point correlation functions follows the same logic and is essentially done by calculating cumulants and using the cyclic properties of the trace. This can e.g. be found in [5].
The equal time Green function $G_{\mathbf{s}}(\theta)_{x,y}$ at $x, y$ and "time" $\theta$ is defined as

$$G_{\mathbf{s}}(\theta)_{x,y} = \langle c_x(\theta) c_y^\dagger(\theta) \rangle \equiv \langle c_x c_y^\dagger \rangle \; . \tag{4.10}$$

Using the matrix notation [6] $\mathbf{A}^{x,y}_{x_1,y_1} = \delta_{x_1,x}\delta_{y_1,y}$ this becomes:

$$(1 - G_{\mathbf{s}}(\theta)) = \langle c_x^\dagger c_y \rangle = \langle \mathbf{c}^\dagger \mathbf{A}^{x,y}_{x_1,y_1} \mathbf{c} \rangle \; . \tag{4.11}$$

One also needs

$$\frac{\partial}{\partial \lambda} \ln \langle \Psi_T | U_1 e^{\lambda O} U_2 | \Psi_T \rangle |_{\lambda=0} = \frac{\langle \Psi_T | U_1 \; O \; U_2 | \Psi_T \rangle}{\langle \Psi_T | U_1 U_2 | \Psi_T \rangle} \; . \tag{4.12}$$

Putting all things together, (4.11) finally reads

$$\begin{aligned}
\langle c_x^\dagger c_y \rangle_{\mathbf{s}} &= \frac{\partial}{\partial \lambda} \ln \langle \Psi_T | U_{\mathbf{s}}(2\theta, \theta) e^{\lambda \mathbf{c}^\dagger \mathbf{A}^{x,y}_{x_1,y_1} \mathbf{c}} U_{\mathbf{s}}(\theta, 0) | \Psi_T \rangle |_{\lambda=0} \\
&= \frac{\partial}{\partial \lambda} \ln det \left[ \mathbf{P}^\dagger B_{\mathbf{s}}(2\theta, \theta) e^{\lambda \mathbf{c}^\dagger \mathbf{A}^{x,y}_{x_1,y_1} \mathbf{c}} B_{\mathbf{s}}(\theta, 0) \mathbf{P} \right]_{\lambda=0} \\
&= \frac{\partial}{\partial \lambda} Tr \ln \left[ \mathbf{P}^\dagger B_{\mathbf{s}}(2\theta, \theta) e^{\lambda \mathbf{c}^\dagger \mathbf{A}^{x,y}_{x_1,y_1} \mathbf{c}} B_{\mathbf{s}}(\theta, 0) \mathbf{P} \right]_{\lambda=0} \\
&\overset{detA = e^{Tr \ln A}}{=} Tr \left[ \frac{\mathbf{P}^\dagger B_{\mathbf{s}}(2\theta, \theta) \mathbf{A}^{x,y}_{x_1,y_1} B_{\mathbf{s}}(\theta, 0) \mathbf{P}}{\mathbf{P}^\dagger \underbrace{B_{\mathbf{s}}(2\theta, \theta) B_{\mathbf{s}}(\theta, 0)}_{B_{\mathbf{s}}(2\theta, 0)} \mathbf{P}} \right] \\
&= \Big( B_{\mathbf{s}}(\theta, 0) \mathbf{P} (\mathbf{P}^\dagger B_{\mathbf{s}}(2\theta, 0) \mathbf{P})^{-1} \mathbf{P}^\dagger B_{\mathbf{s}}(2\theta, \theta) \Big)_{x,y} \\
&= B^> (B^< B^>)^{-1} B^< \\
&= (1 - G_{\mathbf{s}}(\theta))_{x,y} \; .
\end{aligned} \tag{4.13}$$

In line five the cyclic invariance of the trace was used and then the trace was computed explicitly. In line six the following abbreviations were established:

$$B^> = B_{\mathbf{s}}(\theta, 0) \mathbf{P}, \quad B^< = \mathbf{P}^\dagger B_{\mathbf{s}}(2\theta, \theta) \; . \tag{4.14}$$

With the same arguments one also obtains

$$\begin{aligned}
\langle c_{x_2}^\dagger c_{y_2} c_{x_1}^\dagger c_{y_1} \rangle_{\mathbf{s}} &= \langle \langle c_{x_2}^\dagger c_{y_2} c_{x_1}^\dagger c_{y_1} \rangle \rangle_{\mathbf{s}} + \langle c_{x_2}^\dagger c_{y_2} \rangle_{\mathbf{s}} \langle c_{x_1}^\dagger c_{y_1} \rangle_{\mathbf{s}} \\
&= \langle c_{x_2}^\dagger c_{y_1} \rangle_{\mathbf{s}} \langle c_{x_1}^\dagger c_{y_1} \rangle_{\mathbf{s}} + \langle c_{x_2}^\dagger c_{y_2} \rangle_{\mathbf{s}} \langle c_{y_2} c_{x_1}^\dagger \rangle_{\mathbf{s}} \; .
\end{aligned} \tag{4.15}$$

### 4.2.2 Imaginary time displaced Green function $G(\tau\prime, \tau)$

In case of $\tau_1 \geq \tau_2$ the time displaced Green function at $x, y$ is

$$G_{\mathbf{s}}(\tau_1, \tau_2)_{x,y} = \langle c_x(\tau_1) c_y^\dagger(\tau_2) \rangle_{\mathbf{s}} \; . \tag{4.16}$$

One may depict the time displaced Green function like this: a particle is created at time $\tau_2$ with $c_y^\dagger(\tau_2)$, it propagates during the period $\tau_1 - \tau_2$ and is annihilated at a later time $\tau_1$. In order to write down the Green function for a fixed HS field we use the general expression (4.9):

$$\begin{aligned}
G_{\mathbf{s}}(\tau_1, \tau_2)_{x,y} &= \frac{\langle \Psi_T | U_{\mathbf{s}}(2\theta, \tau_1) \hat{c}_x U_{\mathbf{s}}(\tau_1, \tau_2) \hat{c}_y^\dagger U_{\mathbf{s}}(\tau_2, 0) | \Psi_T \rangle}{\langle \Psi_T | U_{\mathbf{s}}(2\theta, 0) | \Psi_T \rangle} \\
&= \frac{\langle \Psi_T | \overbrace{U_{\mathbf{s}}(2\theta, \tau_1) U_{\mathbf{s}}(\tau_1, \tau_2)}^{U_{\mathbf{s}}(2\theta, \tau_2)} \overbrace{(U_{\mathbf{s}}(\tau_1, \tau_2))^{-1} \hat{c}_x U_{\mathbf{s}}(\tau_1, \tau_2)}^{(B_{\mathbf{s}}(\tau_1, \tau_2)\mathbf{c})_x} \hat{c}_y^\dagger U_{\mathbf{s}}(\tau_2, 0) | \Psi_T \rangle}{\langle \Psi_T | U_{\mathbf{s}}(2\theta, 0) | \Psi_T \rangle} \\
&= \frac{\langle \Psi_T | U_{\mathbf{s}}(2\theta, \tau_2) (B_{\mathbf{s}}(\tau_1, \tau_2)\mathbf{c})_x \hat{c}_y^\dagger U_{\mathbf{s}}(\tau_2, 0) | \Psi_T \rangle}{\langle \Psi_T | U_{\mathbf{s}}(2\theta, 0) | \Psi_T \rangle} \\
&= B_{\mathbf{s}}(\tau_1, \tau_2)_{x,z} \, \frac{\langle \Psi_T | U_{\mathbf{s}}(2\theta, \tau_2) \hat{c}_z \hat{c}_y^\dagger U_{\mathbf{s}}(\tau_2, 0) | \Psi_T \rangle}{\langle \Psi_T | U_{\mathbf{s}}(2\theta, 0) | \Psi_T \rangle} \\
&= [B_{\mathbf{s}}(\tau_1, \tau_2) \; G_{\mathbf{s}}(\tau_2)]_{x,y} \; .
\end{aligned} \tag{4.17}$$

The step from line two to line three which introduces the relation

$$(U_{\mathbf{s}}(\tau_1, \tau_2))^{-1} c_x U_{\mathbf{s}}(\tau_1, \tau_2) = (B_{\mathbf{s}}(\tau_1, \tau_2)\mathbf{c})_x \tag{4.18}$$

is made plausible with the following arguments:

1. $U$ is basically composed of one-body operators of the form $e^{-\tau \mathbf{c}^\dagger \mathbf{M} \mathbf{c}}$ ($\mathbf{M}$ shall be an arbitrary matrix) which are applied successively.

2. To evaluate $(U_{\mathbf{s}}(\tau_1, \tau_2))^{-1} c_x U_{\mathbf{s}}(\tau_1, \tau_2)$ we consider the innermost element, i.e. $e^{\tau \mathbf{c}^\dagger \mathbf{M} \mathbf{c}} c_x e^{-\tau \mathbf{c}^\dagger \mathbf{M} \mathbf{c}} = c_x(\tau)$ and then apply the operators of the remaining time slices from the left and right side, respectively.

3. The innermost element fulfills $\frac{\partial}{\partial \tau} c_x(\tau) = -\sum_z \mathbf{M}_{x,z} c_z(\tau)$ and therefore $c_x(\tau) = (e^{-\mathbf{M}})_x$, since

$$\frac{\partial}{\partial \tau} c_x(\tau) = \frac{\partial}{\partial \tau} e^{\tau \mathbf{c}^\dagger \mathbf{M} \mathbf{c}} c_x e^{-\tau \mathbf{c}^\dagger \mathbf{M} \mathbf{c}} = e^{\tau \mathbf{c}^\dagger \mathbf{M} \mathbf{c}} [\mathbf{c}^\dagger \mathbf{M} \mathbf{c}, c_x] e^{-\tau \mathbf{c}^\dagger \mathbf{M} \mathbf{c}} \; . \tag{4.19}$$

After evaluating the commutator

$$\begin{aligned}
[\mathbf{c}^\dagger \mathbf{M}\mathbf{c}, c_x] &= \sum_{i,j} M_{i,j}[c_i^\dagger c_j, c_x] \\
&= \sum_{i,j} M_{i,j}(-c_i^\dagger c_x c_j - c_i^\dagger c_j c_x) \\
&= \sum_{i,j} M_{i,j}(-(\delta_{x,i} - c_x c_i^\dagger)c_j - c_i^\dagger c_j c_x) \\
&= -\sum_{i,j} M_{i,j}\delta_{x,i}c_j = -\sum_j M_{x,j}c_j
\end{aligned}$$

one obtains

$$\begin{aligned}
\frac{\partial}{\partial\tau}c_x(\tau) &= e^{\tau\mathbf{c}^\dagger\mathbf{M}\mathbf{c}}(-\sum_j M_{x,j}c_j)e^{-\tau\mathbf{c}^\dagger\mathbf{M}\mathbf{c}} \\
&= -\sum_j M_{x,j}c_j(\tau). \qquad (4.20)
\end{aligned}$$

Therefore (4.18) is justified. Since the propagator $B_{\mathbf{s}}(\tau_1, \tau_2)$ is a matrix one can pull it out of the sum, which is how we go from line four to line five in (4.17).

For time displaced Green function a Wick theorem equally holds, a proof may found in [6]. In conclusion, the time displaced Green function is obtained upon propagation that is matrix multiplication from the left on the equal time Green function. Although mathematically exact, this kind of propagation cannot be implemented readily into the algorithm since instabilities will develop at large times that is after many multiplications. A central task is therefore to find a efficient method to calculate time displaced Green functions.

### 4.2.3 Efficient calculation of $G(\tau\prime, \tau)$

The knowledge of the imaginary-time displaced Green function for different parameters of the lattice system allows to extract valuable information about spin and charge gaps or quasiparticle weights. Dynamical properties like the single particle spectral function can also be obtained after analytic continuation to real time.
For the free system, $G(\tau, 0)$ can be calculated analytically, following Chapter 2,

$$\begin{aligned}
G_{\mathbf{k}}(\tau, 0) &= \langle \hat{c}_{\mathbf{k}}(\tau)\hat{c}_{\mathbf{k}}^\dagger(0)\rangle \\
&= \frac{1}{2}\Big(\langle \hat{\gamma}_{\mathbf{k}}(\tau)\hat{\gamma}_{\mathbf{k}}^\dagger(0)\rangle + \langle \hat{\eta}_{\mathbf{k}}(\tau)\hat{\eta}_{\mathbf{k}}^\dagger(0)\rangle\Big) \\
&= \frac{1}{2}\Big(e^{-\tau E_\gamma(\mathbf{k})}\langle \hat{\gamma}_{\mathbf{k}}\hat{\gamma}_{\mathbf{k}}^\dagger\rangle + e^{-\tau E_\eta(\mathbf{k})}\langle \hat{\eta}_{\mathbf{k}}\hat{\eta}_{\mathbf{k}}^\dagger\rangle\Big) \\
&\overset{T\to 0}{=} \frac{1}{2}e^{-\tau\Gamma(\mathbf{k})}\,. \qquad (4.21)
\end{aligned}$$

The last line follows with $E_{\gamma,\eta}(\mathbf{k}) = \mp\Gamma(\mathbf{k})$. In the general case the imaginary time displaced Green function is a superposition of many exponential functions of different frequencies, corresponding to the excitation energies of the $(N+1)$- particle system with respect to the $N$-particle ground state $|\Psi_0^N\rangle$:

$$\begin{aligned} G_{\mathbf{k}}(\tau,0) &\overset{\tau\geq 0}{=} \langle \hat{c}(\tau)\hat{c}^\dagger(0)\rangle \\ &= \langle \Psi_0^N | e^{\tau H}\hat{c}e^{-\tau H}\hat{c}^\dagger|\Psi_0^N\rangle \\ &= \sum_{\Psi_0^{N+1}} \langle \Psi_0^N | e^{\tau H}\hat{c}e^{-\tau H}|\Psi_0^{N+1}\rangle\langle\Psi_0^{N+1}|\hat{c}^\dagger|\Psi_0^N\rangle \\ &= \sum_{\Psi_0^{N+1}} e^{\tau E_0^N}\langle \Psi_0^N|\hat{c}|\Psi_0^{N+1}\rangle e^{-\tau E_0^{N+1}}\langle\Psi_0^{N+1}|\hat{c}^\dagger|\Psi_0^N\rangle \\ &= \sum_{\Psi_0^{N+1}} |\langle \Psi_0^N|\hat{c}|\Psi_0^{N+1}\rangle|^2 e^{\tau(E_0^N - E_0^{N+1})} \; . \end{aligned} \tag{4.22}$$

In principle and on the paper one would apply (4.17) to compute $G(\tau\prime,\tau)$. In practice we encounter the problem of competing timescales: the time scale $\tau\prime - \tau$ is usually not compatible with the time scale $\tau_{st}$ on which matrix multiplication is numerically stable. Without correction results for large values of $\tau$ will be unreliable [5].
To circumvent this problem, we applied the method suggested by M.Feldbacher and F.F.Assaad [35]. The argument goes like this: the large $\tau\prime - \tau$ interval is broken up into a set of $N$ small intervals of the length $\tau_{st} = (\tau\prime - \tau)/N$. Whenever the time displacement is a multiple of $\tau_{st}$, the equal time Green function at the given time slice, $G(n\tau_{st}, n\tau_{st}), n = 1, \cdots, N-1$ is recomputed in a stable manner and serves as starting point for the next time evolution. This approach is based on the observation, that

$$G_{\mathbf{s}}(\tau,\tau)^2 = G_{\mathbf{s}}(\tau,\tau) \; . \tag{4.23}$$

Thus, for a fixed auxilliary field the equal time Green function is a projector. This can be proven by conducting a singular value decomposition (SDV) of the matrix $G_{\mathbf{s}}(\tau,\tau)$, see section 5.2 for the proof of (4.23). Following [35], a composition property for $G_{\mathbf{s}}(\tau_3,\tau_1)$ holds:

$$\begin{aligned} G_{\mathbf{s}}(\tau_3,\tau_1) &= B_{\mathbf{s}}(\tau_3,\tau_1)G_{\mathbf{s}}(\tau_1,\tau_1) \\ &= B_{\mathbf{s}}(\tau_3,\tau_1)G_{\mathbf{s}}(\tau_1,\tau_1)^2 \\ &= G_{\mathbf{s}}(\tau_3,\tau_1)G_{\mathbf{s}}(\tau_1,\tau_1) \\ &= G_{\mathbf{s}}(\tau_3,\tau_1)\Big(B_{\mathbf{s}}(\tau_2,\tau_1)\Big)^{-1}B_{\mathbf{s}}(\tau_2,\tau_1)G_{\mathbf{s}}(\tau_1,\tau_1) \\ &= G_{\mathbf{s}}(\tau_3,\tau_2)G_{\mathbf{s}}(\tau_2,\tau_1) \; . \end{aligned} \tag{4.24}$$

In general, given a time interval $\tau$ of length $\tau = N\tau_{st}$ we obtain:

$$\begin{aligned} G_{\mathbf{s}}(\theta+\tau,\theta) &= G_{\mathbf{s}}(\theta+\tau,\theta+\tau-\tau_{st})\cdots G_{\mathbf{s}}(\theta+2\tau_{st},\theta+\tau_{st})G_{\mathbf{s}}(\theta+\tau_{st},\theta) \\ &= \prod_{n=0}^{N-1} G_{\mathbf{s}}(\theta+[n+1]\tau_{st},\theta+n\tau_{st}) \ . \end{aligned} \tag{4.25}$$

In the product above each Green function extends over an imaginary time interval of $\tau_{st}$ and can therefore be computed accurately via matrix multiplication.

# 5 Outline of the Monte Carlo Technique

The Monte Carlo method is a stochastical process to obtain the expectation value $\langle A \rangle$ of an observable $A$ at in principle arbitrary precision with error bars included. As it has been argued in the last chapter the principle quantity to evaluate expectation values is the partition function. This quantity can be calculated exactly (except for the Trotter error from discretization of order $\Delta\tau^2$) in the case that all configurations of the auxilliary fields are known. The goal of the Monte Carlo technique is to chose from all possible configurations those $N$-parts which enter the partition function with a significant weight. Having done this, the observable is calculated for each of these configurations and the mean value is formed. This procedure is repeated several times, each time with a new that is independent set of highly probable configurations. According to the central limit theorem the thus obtained mean values are normal distributed around the exact expectation value of the observable.
In order to implement the Monte Carlo method in the algorithm one has to find a way to extract the weight $P_s$ which belongs to each configuration. As it will be shown this weight can be formulated with the equal time Green function. Therefore the Green function is the decisive entity in choosing of configurations that is in the update procedure.

## 5.1 The Monte Carlo sampling

The challenge lies in the numerical calculation of the integral

$$\langle A \rangle = \int_\Omega d\vec{s} P(\vec{s}) A(\vec{s}) \tag{5.1}$$

over the configuration space $\Omega$. The probability distribution $P(\vec{s})$, with $\int_\Omega d\vec{s} P(\vec{s}) = 1$ and $P(\vec{s}) \geq 0 \; \forall \vec{s} \in \Omega$, is of course not known. Starting from a random configuration of the HS-field $\vec{s}$ it is nevertheless possible to arrive at a sequence of configurations which are distributed according to the probability $P(\vec{s})$. A configuration of the HS-field $\vec{s}$ is determined by Ising spins on all lattice sites and time slices. Figuratively one can think of the HS-field in the case of two spatial dimensions as a three dimensional matrix consisting of a two dimensional lattice on each time slice and each lattice site is occupied by an up or down spin. Let us assume that we already have a set of field configurations $\{\vec{s}_1, \vec{s}_2, \cdots, \vec{s}_N\}$ being distributed according to $P(\vec{s})$. Then the integral (5.1) can be evaluated approximately

as

$$\langle A \rangle \approx \frac{1}{N} \sum_{i=1, \vec{s}_i \in P(\vec{s})}^{N} A(\vec{s}_i) \; . \tag{5.2}$$

In the case of many and mutually independent sets $\{\{\vec{s}_{1,i}\}, \{\vec{s}_{2,i}\}, \cdots | i = 1 \cdots N\}$ the central limit theorem holds in the limit $N \to \infty$. Thereby one gains the mean value with a statistical value according to the width $\sigma$ of the Gaussian distribution.
We understand the unknown and sought-after distribution $P(\vec{s})$ as the equilibrium distribution of a Markov process. The Markov chain of first order is defined with a discrete Monte Carlo time $t$ like this: the future only depends on the present that is the state of the system at $t+1$ only follows from its state at $t$ and in particular is conditionally independent of the past. The Markov chain is determined by a transition matrix $T_{\vec{s}_2, \vec{s}_1}$ which describes the transition probability $\vec{s}_1 \to \vec{s}_2$. $T$ is assumed to be ergodic and suitably normalized. Therefore the time evolution of the distribution reads [6]

$$P(\vec{s}_2)_{t+1} = \sum_{s_1} T_{\vec{s}_2, \vec{s}_1} P(\vec{s}_1)_t \tag{5.3}$$

The equilibrium distribution $P(\vec{s})$, defined as $P(\vec{s})_{t \to \infty} = P(\vec{s})$ fulfills the condition of detailed balance

$$T_{\vec{s}_2, \vec{s}_1} P(\vec{s}_1) = T_{\vec{s}_1, \vec{s}_2} P(\vec{s}_2). \tag{5.4}$$

To go from configuration $\vec{s}_1$ to configuration $\vec{s}_2$ a single spin flip algorithm is used. This means that the flipping probability is calculated for every single point $s_{i,n}$ of the discrete field $\vec{s}_1$, characterized by a spatial coordinate $i$ and the imaginary time coordinate $n$. The decision on acceptance or denial of a spin flip is based on the flipping probability and is done stochastically, e.g. with a Metropolis scheme (in the appendix). Like this one sweeps through the whole lattice in space and time and creates a Markov chain of configurations. Naturally two consecutive configurations are highly correlated since at maximum (in the case of acceptance) one of the $N \times n$ spins was altered. Generally the autocorrelation function $C_A(t)$ of the observable $A$ can be assumed to be exponentially falling, $C_A(t) \propto e^{-t/\tau_0}$. Here $\tau_0$ determines the time scale after which a configuration independent from the starting configuration is reached. The autocorrelation time $\tau_0$ is usually dependent of the individual observables and the concomitant symmetries of the Hamiltonian.
In order to apply the central limit theorem we introduce the terms *sweep* and *bin* which allows us to reformulate (5.2):

$$A_{bin} = \frac{1}{N} \sum_{i=1}^{N} A_{sweep}(\vec{s}_{t=\tau_0 \cdot i}) \; . \tag{5.5}$$

Thus we measure the Observable on $N$ conditionally independent configurations at distance $\tau_0$ and regroup the individual measurements to the mean value $A_{bin}$. Several mutually independent mean values $A_{bin}(t_{bin})$, $t_{bin} = 1, \cdots M$ are defined equally as

$$A_{bin}(t_{bin}) = \frac{1}{N} \sum_{i=1}^{N} A_{sweep}(\vec{s}_{t=\tau_0 \cdot i + (t_{bin}-1)N\tau_0}) \; . \tag{5.6}$$

The error of the expectation value obtained from the $M$ mean values $A_{bin}$ is given by the variance $\sigma = \sqrt{\langle A_{bin}^2 \rangle - \langle A_{bin} \rangle^2}$. In the present work the error analysis was however done with an alternative method, called the *jackknife* error analysis. This technique allows to determine the errors of functions which depend on several observables [9].

### 5.1.1 Implementation in the algorithm

According to (4.9), an observable $A$ in the PQMC algorithm is computed via

$$\langle A \rangle = \sum_{\mathbf{s}} P_{\mathbf{s}} \, \langle A \rangle_{\mathbf{s}} \; . \tag{5.7}$$

The weight $P_{\mathbf{s}}$ of an time slice (index $n$) and lattice site (index $\mathbf{i}$) dependent field configuration $\mathbf{s} = s_{\mathbf{i},n}$ is

$$P_{\mathbf{s}} = \frac{det[\mathbf{P}^\dagger B_{\mathbf{s}}(2\theta,0)\mathbf{P}]}{\sum_{\mathbf{s}} \langle \Psi_T | U_{\mathbf{s}}(2\theta,0) | \Psi_T \rangle} \tag{5.8}$$

As mentioned above, to move form a given configuration $\mathbf{s}$ to the next configuration $\mathbf{s\prime}$, we make a single spin flip decision. This decision is governed by the ratio

$$R = \frac{P_{\mathbf{s\prime}}}{P_{\mathbf{s}}} = \frac{det[\mathbf{P}^\dagger B_{\mathbf{s\prime}}(2\theta,0)\mathbf{P}]}{det[\mathbf{P}^\dagger B_{\mathbf{s}}(2\theta,0)\mathbf{P}]} \tag{5.9}$$

A single spin flip means a change in the imaginary time propagator $B(2\theta,0)$ (3.19), more precisely the interaction term $e^{V(\mathbf{s}_n)}$ is altered to $e^{V(\mathbf{s\prime}_n)}$. Following [5] this term can be written as

$$e^{V(\mathbf{s\prime}_n)} = \Big(1 + [e^{V(\mathbf{s\prime}_n)} e^{-V(\mathbf{s}_n)} - 1]\Big) e^{V(\mathbf{s}_n)} = \Big(1 + \Delta\Big) e^{V(\mathbf{s}_n)} \; . \tag{5.10}$$

The new propagator is therefore

$$\begin{aligned} B_{\mathbf{s\prime}}(2\theta,0) &= \prod_{n=1}^{m} e^{\mathbf{V}(\mathbf{s\prime}_n)} e^{-\Delta\tau\mathbf{T}} \\ &= B_{\mathbf{s\prime}}(2\theta,\tau) B_{\mathbf{s\prime}}(\tau,0) \\ &= \overbrace{e^{\mathbf{V}(\mathbf{s\prime}_m)} e^{-\Delta\tau\mathbf{T}} \cdots e^{\mathbf{V}(\mathbf{s\prime}_{n+1})} e^{-\Delta\tau\mathbf{T}}}^{B_{\mathbf{s\prime}}(2\theta,\tau)} \overbrace{e^{\mathbf{V}(\mathbf{s\prime}_n)} e^{-\Delta\tau\mathbf{T}} \cdots e^{\mathbf{V}(\mathbf{s\prime}_1)} e^{-\Delta\tau\mathbf{T}}}^{B_{\mathbf{s\prime}}(\tau,0)} \\ &= e^{\mathbf{V}(\mathbf{s\prime}_m)} e^{-\Delta\tau\mathbf{T}} \cdots e^{\mathbf{V}(\mathbf{s\prime}_{n+1})} e^{-\Delta\tau\mathbf{T}} \Big(1 + \Delta\Big) e^{V(\mathbf{s}_n)} e^{-\Delta\tau\mathbf{T}} \cdots e^{\mathbf{V}(\mathbf{s\prime}_1)} e^{-\Delta\tau\mathbf{T}} \\ &= B_{\mathbf{s}}(2\theta,\tau) \Big(1 + \Delta\Big) B_{\mathbf{s}}(\tau,0) \end{aligned} \tag{5.11}$$

with $2\theta = m\Delta\tau$. This allows us to rewrite the ratio $R$ [5] to

$$\begin{aligned} R &= \frac{det[\mathbf{P}^\dagger B_{\mathbf{s}\prime}(2\theta,0)\mathbf{P}]}{det[\mathbf{P}^\dagger B_{\mathbf{s}}(2\theta,0)\mathbf{P}]} \\ &= \frac{det[\mathbf{P}^\dagger B_{\mathbf{s}}(2\theta,\tau)\Big(1+\Delta\Big)B_{\mathbf{s}}(\tau,0)\mathbf{P}]}{det[\mathbf{P}^\dagger B_{\mathbf{s}}(2\theta,0)\mathbf{P}]} \\ &= \frac{det[B^<_{\mathbf{s}}\Big(1+\Delta\Big)B^>_{\mathbf{s}}]}{det[B^<_{\mathbf{s}}B^>_{\mathbf{s}}]} \\ &= det[B^<_{\mathbf{s}}\Big(1+\Delta\Big)B^>_{\mathbf{s}}\Big(B^<_{\mathbf{s}}B^>_{\mathbf{s}}\Big)^{-1}] \\ &= det[1+B^<_{\mathbf{s}}\Delta B^>_{\mathbf{s}}\Big(B^<_{\mathbf{s}}B^>_{\mathbf{s}}\Big)^{-1}] \\ &= det[1+\Delta B^>_{\mathbf{s}}\Big(B^<_{\mathbf{s}}B^>_{\mathbf{s}}\Big)^{-1}B^<_{\mathbf{s}}] \\ &= det[1+\Delta\Big(1-G_{\mathbf{s}}(\tau)\Big)]\,, \end{aligned} \tag{5.12}$$

The ratio of the probability weights $P_{\mathbf{s}}$ and $P_{\mathbf{s}\prime}$ is thus completely determined by the matrix $\Delta$ and the equal time Green function $G_{\mathbf{s}}(\tau)$. In other words, to compute $R$ for two neighbouring configurations, $\mathbf{s}$ and $\mathbf{s}\prime$, we have to compute the Green function of $\mathbf{s}$.
If the spin flip is accepted, the Green function has to be recomputed:

$$G_{\mathbf{s}\prime}(\tau) = 1 - \Big(1+\Delta\Big)B^>_{\mathbf{s}}\left(B^<_{\mathbf{s}}\Big(1+\Delta\Big)B^>_{\mathbf{s}}\right)^{-1}B^<_{\mathbf{s}} \tag{5.13}$$

Since $G_{\mathbf{s}\prime}(\tau)$ differs form $G_{\mathbf{s}}(\tau)$ only by the matrix $\Delta$, which has a few non-zero components, computational effort can be greatly reduced by applying a matrix inversion technique, the Sherman-Morrison formula [9].
To sum up, we have shown how the Monte-Carlo approach can be implemented in the PQMC algorithm. Observables are measured on a series of field configurations which are regarded to be distributed according to the equilibrium distribution. Configurations are generated, starting from a completely random Ising field, on the basis of a single spin flip scheme.

## 5.2 The PQMC algorithm

This section concludes the technical part by summarizing the essential steps of the computer algorithm and its practical realization. Some formula although itself correct on the paper cannot be transfered one-to-one to the program. This is due to finite precision of the numbers being processed and competing scales which without correction result in a loss of information. Stabilization schemes therefore constitute a vital part of numerical calculations. One technique, the singular value decomposition (SDV) is extensively used

within the algorithm. Here we sketch the main idea and refer for a more profound explanation to the appendix.
SDV deals with matrices which are numerically close to singular, that is with matrices which are close to be non-invertible. In our case this happens to the propagated wave function: we start with a trial wave function, the Slater determinant (4.4), which is characterized by the matrix $\mathbf{P}$. $\mathbf{P}$ consists of $N_p$ (number of particles) orthonormal column vectors the entries of which are distributed among the $N_S$ single particle states. To approximate the unknown ground state wave function, $\mathbf{P}$ is projected along the imaginary time axis. This is done by the propagator $B(\tau, 0)$, which is essentially a matrix multiplication with exponential factors. After the time $\tau$ the propagated wave function $B(\tau, 0)\mathbf{P}$ will be dominated by the large scales of $B(\tau, 0)$ at the expense of the small scales. When $\tau$ is big this may result in two or more column vectors of $B(\tau, 0)\mathbf{P}$ being almost the same, in other words the determinant is zero and the matrix non-invertible.
To avoid numerically ill-conditioned matrices the matrix has to be recomputed on a regular basis. The stabilization, more precisely the orthogonalization is accomplished by SDV. The unique feature of SDV lies in the fact that it leaves the equal time Green function, the building block of the whole algorithm invariant. The line of reasoning goes like this: the matrix $B^{>} = B(\tau, 0)\mathbf{P}$ is decomposed in a set of three matrices of a certain shape, which is mathematically exact (see the appendix),

$$B^{>} = U^{>} D_R V_R \,. \tag{5.14}$$

The essential information is enclosed in $U^{>}$: its $N_P$ column vectors are obtained from the column vectors of the original matrix $B^{>}$ through orthogonalization and normalization. Since the same processing can be applied to $B^{<} = \mathbf{P}^{\dagger} B(2\theta, \tau) = V_L D_L U^{<}$, the Green function (4.13) is [5]

$$\begin{aligned} 1 - G(\tau) &= B^{>}\Big(B^{<}B^{>}\Big)^{-1} B^{<} \\ &= U^{>} D_R V_R \Big(V_L D_L U^{<} U^{>} D_R V_R\Big)^{-1} V_L D_L U^{<} \\ &= U^{>} D_R V_R \Big(D_R V_R\Big)^{-1} \Big(U^{<} U^{>}\Big)^{-1} \Big(V_L D_L\Big)^{-1} V_L D_L U^{<} \\ &= U^{>}\Big(U^{<} U^{>}\Big)^{-1} U^{<} \,. \end{aligned} \tag{5.15}$$

Thus, the important information to compute the Green function is solely encoded in the $U^{>}$, $U^{<}$ matrices. Given this decomposition property we can easily show that the equal

time Green function is a projector,

$$\begin{aligned} G_{\mathbf{s}}(\tau)^2 &= \left(1 - U_{\mathbf{s}}^{>}\left(U_{\mathbf{s}}^{<}U_{\mathbf{s}}^{>}\right)^{-1}U_{\mathbf{s}}^{<}\right)^2 \\ &= 1 - 2U_{\mathbf{s}}^{>}\left(U_{\mathbf{s}}^{<}U_{\mathbf{s}}^{>}\right)^{-1}U_{\mathbf{s}}^{<} + U_{\mathbf{s}}^{>}\underbrace{\left(U_{\mathbf{s}}^{<}U_{\mathbf{s}}^{>}\right)^{-1}U_{\mathbf{s}}^{<}U_{\mathbf{s}}^{>}}_{=\mathbf{1}}\left(U_{\mathbf{s}}^{<}U_{\mathbf{s}}^{>}\right)^{-1}U_{\mathbf{s}}^{<} \\ &= 1 - U_{\mathbf{s}}^{>}\left(U_{\mathbf{s}}^{<}U_{\mathbf{s}}^{>}\right)^{-1}U_{\mathbf{s}}^{<} \\ &= G_{\mathbf{s}}(\tau)\ . \end{aligned} \tag{5.16}$$

### 5.2.1 Efficient realization

An efficient implementation of the PQMC algorithm should result in a small warm-up phase and low autocorrelation times. This assures that many valid measurements can be taken which are both independent of each other and - to reflect the particle interaction correctly - rely on a valid configuration of auxilliary fields. In the following we sketch the essential steps leading to a fast and stable algorithm [5].
As mentioned before, the pivotal quantity is the equal time Green function $G_{\mathbf{s}}(\tau)$,

$$\begin{aligned} G_{\mathbf{s}}(\tau) &= 1 - \prod_{n=1}^{n_\tau} e^{\mathbf{V}(\mathbf{s}_n)}e^{-\Delta\tau\mathbf{T}}\mathbf{P}\left(\mathbf{P}^\dagger\prod_{n=1}^{m} e^{\mathbf{V}(\mathbf{s}_n)}e^{-\Delta\tau\mathbf{T}}\mathbf{P}\right)^{-1}\mathbf{P}^\dagger\prod_{n=n_\tau+1}^{m} e^{\mathbf{V}(\mathbf{s}_n)}e^{-\Delta\tau\mathbf{T}} \\ &= 1 - B_{\mathbf{s}}^{>}\left(B_{\mathbf{s}}^{<}B_{\mathbf{s}}^{>}\right)^{-1}B_{\mathbf{s}}^{<} \\ &= 1 - U_{\mathbf{s}}^{>}\left(U_{\mathbf{s}}^{<}U_{\mathbf{s}}^{>}\right)^{-1}U_{\mathbf{s}}^{<} \end{aligned} \tag{5.17}$$

At this point it is appropriate to clarify on the use of the field variable $\mathbf{s}$. Generally spoken, there is an independent HS field for each lattice site $\mathbf{i}$ and time slice $n$. Those individual fields take the values $\pm 1$ and are subject to the single spin flip decisions as discussed above. That is every field fluctuates in Monte Carlo time between the values $\pm 1$. The matrix $\mathbf{P}$ is propagated along the imaginary time axis and at each time slice $n$ a sweep through the lattice is made resulting in a new configuration on that time slice. This configuration is denoted by the index $\mathbf{s}_n$. The Green function $G_{\mathbf{s}}(\tau)$ at any given time $\tau$ being a non-local function relies on the entirety of fields i.e on the momentary values of $N \times m$ field variables, which is indicated by the index $\mathbf{s}$.

During the simulation a specified number of sweeps are done each of which consists of a downward run from $\tau = 2\theta$ to $\tau = \Delta\tau$ and a subsequent upward run from $\tau = \Delta\tau$ to $\tau = 2\theta$. In the course of propagation the SDV stabilization scheme is applied periodically. The total imaginary time interval $2\theta = m\Delta\tau$ is thus segmented into $n$ sub-intervals of length $\tau_1$ such that $n\tau_1 = 2\theta$. This is shown schematically in Fig.5.1.

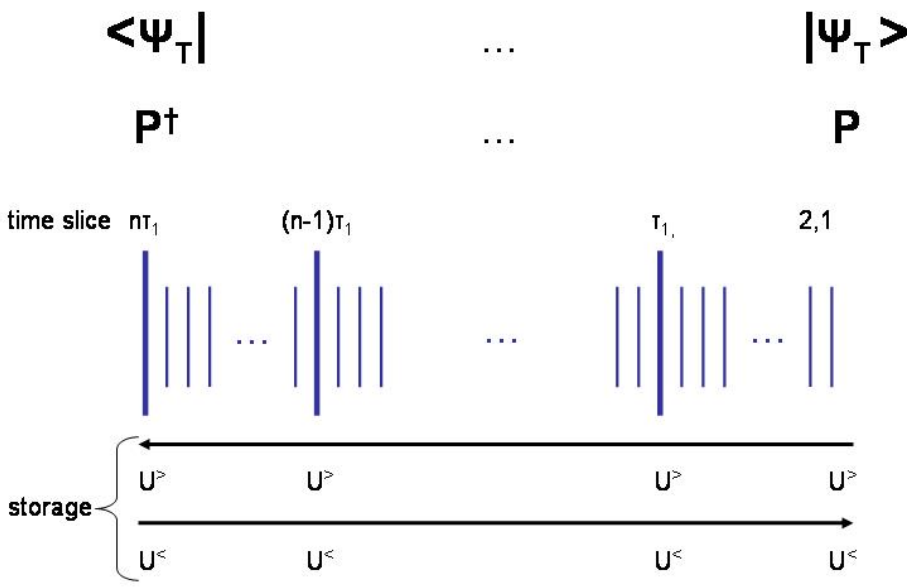


**Figure 5.1:** Schematic illustration of the updating and storage procedure. The projector matrix $\mathbf{P}$ ($\mathbf{P}^\dagger$) is propagated via matrix multiplication along the imaginary time axis in the upward (downward) direction. The Green function at time slices $\tau_1, \cdots n\tau_1$ which requires both $U^>$ and $U^<$ is obtained by orthonormalizing the $U$-matrix ($U^>$ or $U^<$, depending on direction of propagation) and reading its counterpart from the storage. The same storage slot is then filled with the $U$-matrix to be used in the following run.

To save computer time we store the matrices $U^{<}_{n_\tau}$ (downward move) and $U^{>}_{n_\tau}$ (upward move) each time they have been calculated. This gives us a fresh estimate of the Green function every $\tau_1$ time step: $U^{>}_{n_\tau}$ is read in from the storage slot where it has been stored upon diagonalization at the previous upward run. Together with the just calculated and orthonormalized matrix $U^{<}_{n_\tau}$ it constitutes the Green function $G_{\mathbf{s}}(n_\tau)$ (5.17). $U^{<}_{n_\tau}$ is then stored at the same storage slot for the following upward run to which the same logic applies.
At the beginning of the sweeps a random field $\mathbf{s}_{rnd}$ is used at all time slices and lattices sites and the storage slots are filled with propagations according to the random field. All observables are measured symmetrically around the middle time slice $n = m/2$, usually on the time slices $m/2 - 10, \cdots m/2 + 10$. Since the Green function can be calculated in a stable manner we have access to all observables via Wick's theorem.

# 6 Results

All numerical results presented in this chapter have been obtained with the previously illustrated PQMC algorithm. The general goal was to study the Hubbard model on the honeycomb lattice with different sets of the parameters $U$ and $H$. In the canonical framework of the PQMC simulation the magnetic field $H$ was mimicked by implementing the magnetization $M_z$. The magnetization is altered by varying the number of electrons in the spin-up sector and keeping the total number of elctrons constant. In principle it is possible to obtain the corresponding vertical magnetic field from the vertical magnetization,

$$B = \frac{dE_0}{dM_z} = \frac{E_0(N, M_z + 1) - E_0(N, M_z - 1)}{2} \, . \tag{6.1}$$

Since the numerical effort to obtain well converged Green functions $G(\tau)$ is considerable, dynamic calculations were only done for a $6 \times 6$ lattice. At zero temperature the spectral density can be extracted from the knowledge of the Green function via

$$G_{\mathbf{k}}(\tau) = \langle \hat{c}_{\mathbf{k}}(\tau) \hat{c}^{\dagger}_{\mathbf{k}} \rangle = \int d\omega e^{-\omega\tau} A(\mathbf{k}, \omega) \, . \tag{6.2}$$

Formally, $A(\mathbf{k}, \omega)$ can be obtained with an inverse Laplace transform. However, due to competing scales this inversion is numerically ill-defined. Furthermore, the Green function is in general only known on a set of discrete points in imaginary time.
Instead, to extract spectral data we used the Maximum-Entropy method (MEM), more precisely a stochastic version of MEM. In a nutshell, this method uses an systematic averaging approach to select candidate solutions which are consistent with the data and takes their average [40],[41],[42].

## 6.1 Static observables

The orbital components of the equal time spin-spin correlation function $S^{+-}(\mathbf{k})$ are

$$
\begin{aligned}
S^{+-}_{\mu,\nu}(\mathbf{k}) &= \frac{1}{N^2}\sum_{\mathbf{i},\mathbf{j}} e^{-\imath\mathbf{k}(\mathbf{i}-\mathbf{j})}\langle S^{+}_{\mu,i} S^{-}_{\nu,j}\rangle \\
&= \frac{1}{N^2}\sum_{\mathbf{i},\mathbf{j}} e^{-\imath\mathbf{k}(\mathbf{i}-\mathbf{j})}\langle \hat{c}^{\dagger}_{i,\uparrow}\hat{c}_{i,\downarrow}\hat{c}^{\dagger}_{j,\downarrow}\hat{c}_{j,\uparrow}\rangle \\
&= \frac{1}{N^2}\sum_{\mathbf{i},\mathbf{j}} e^{-\imath\mathbf{k}(\mathbf{i}-\mathbf{j})}\Big(\underbrace{\langle \hat{c}^{\dagger}_{i,\uparrow}\hat{c}_{i,\downarrow}\rangle\langle \hat{c}^{\dagger}_{j,\downarrow}\hat{c}_{j,\uparrow}\rangle}_{=0} + \langle \hat{c}^{\dagger}_{i,\uparrow}\hat{c}_{i,\uparrow}\rangle\langle \hat{c}^{\dagger}_{j,\downarrow}\hat{c}_{j,\downarrow}\rangle\Big) \\
&= \frac{1}{N^2}\sum_{\mathbf{i},\mathbf{j}} e^{-\imath\mathbf{k}(\mathbf{i}-\mathbf{j})}\langle \hat{c}^{\dagger}_{i,\uparrow}\hat{c}_{i,\uparrow}\rangle\langle \hat{c}^{\dagger}_{j,\downarrow}\hat{c}_{j,\downarrow}\rangle \ . \qquad (6.3)
\end{aligned}
$$

To arrive at the third line Wick's theorem was applied and the knowledge that the spin up and spin down channels are factorized[1]. From now on we omit the orbital indices $\mu, \nu$ which indicate the sublattices $A$ and $B$ and take $\mu = \nu = 1$ unless stated otherwise. The transversal magnetization is $m^{+-} = \frac{1}{N}\sqrt{S^{+-}(\mathbf{q})}$ at the ordering vector $\mathbf{q} = (0, 0)$. Measuring the vertical magnetization using the spin-spin correlation function $S^{zz}(\mathbf{k})$ does not give us anything new, since this is what we pluged in in the first place.
In case of half filling on a $L \times L$-lattice with two orbitals on each lattice point there exists a total electron number of $N_{tot} = N_{\uparrow} + N_{\downarrow} = 2L \cdot L$. The magnetization is defined as

$$
M_z = \frac{(N_{\uparrow} - N_{\downarrow})}{(N_{\uparrow} + N_{\downarrow})} = \frac{(N_{\uparrow} - N_{\downarrow})}{2L \cdot L} \ . \qquad (6.4)
$$

The measurements were made on lattices of size $10 \times 10$, $12 \times 12$, $14 \times 14$ and $16 \times 16$. As shown in Fig.6.1 there does not exist a gap at a interaction strength of $U = 2$ but it opens up if $U$ exceeds the critical interaction strength. From Fig.6.2 we expect $U_c$ to be in the range $U_c \approx 4 - 5$. This in agreement with results which were obtained previously [13], [16].

## 6.2 Excitation spectra

We define the Green functions

$$
\begin{aligned}
G_{\mathbf{k},\sigma} &= \langle \hat{c}_{\mathbf{k},\sigma}(\tau)\hat{c}^{\dagger}_{\mathbf{k},\sigma}\rangle \\
\overline{G}_{\mathbf{k},\sigma} &= \langle \hat{c}^{\dagger}_{\mathbf{k},\sigma}(\tau)\hat{c}_{\mathbf{k},\sigma}\rangle \ . \qquad (6.5)
\end{aligned}
$$

In order to get a complete picture of the single particle excitations in general on has to look at both Green functions $G_{\mathbf{k},\sigma}$ and $\overline{G}_{\mathbf{k},\sigma}$. Probing the unoccupied states by inserting a

[1] It is important to note that Wick's theorem holds for a given Hubbard-Stratonovich field only. Its use is however justified here since the observables are computed at a set of distinct Hubbard-Stratonovich configurations.

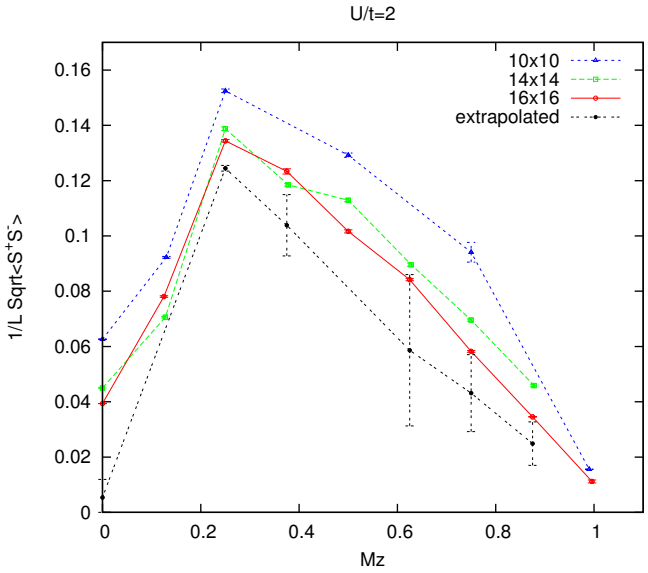


(a) The initial rise of the staggered magnetization is attributed to the nesting property of the lattice whereas its subsequent decrease is a consequence of total polarization.

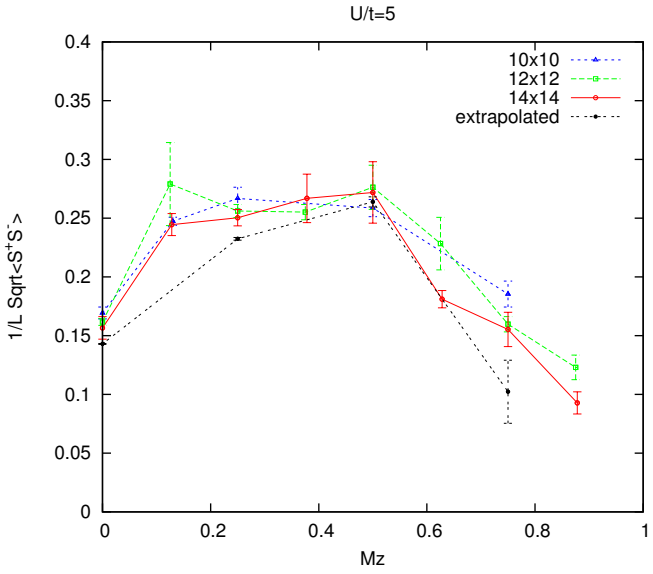


(b) A finite transversal magnetization is observed even at zero external field (at zero vertical magnetization). This indicates a Mott-Hubbard transition with $U_c < 5$.

**Figure 6.1:** Staggered magnetization vs. magnetization $M_z$ for $U < U_c$ and $U > U_c$. Measurements were taken with the projection parameter $\theta = 20$ and with discretization parameter $\Delta\tau = 0.1$. Extrapolations to $1/L \to 0$ were conducted when possible.

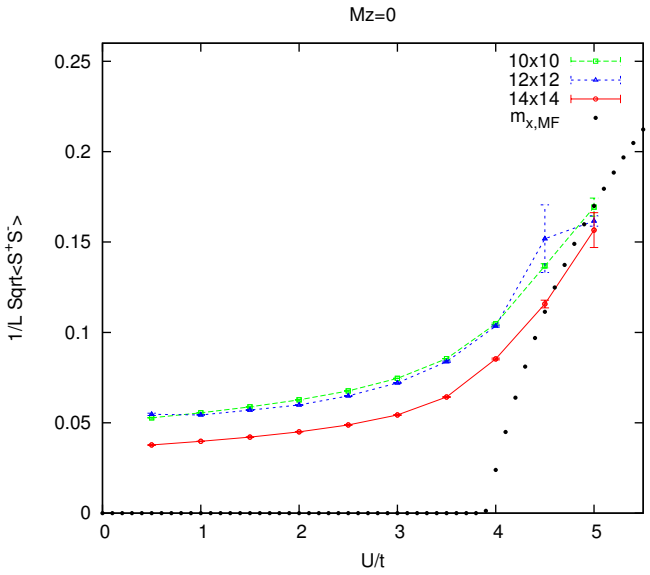


**Figure 6.2:** Staggered magnetization and the mean field parameter $m_{x,MF}$ vs. interaction strength $U$. For comparison, mean-field data is plotted.

particle via $\langle \hat{c}_{\mathbf{k},\sigma}(\tau)\hat{c}^{\dagger}_{\mathbf{k},\sigma}\rangle$ eperimentally corresponds to inverse photoemission spectroscopy (IPES). Likewise photoemission spektroscopy (PES) yields information about the occupied band structure below the chemical potential. In case of half filling $G_{\mathbf{k},\sigma}$ and $\overline{G}_{\mathbf{k},\sigma}$ are linked via a particle-hole transformation. The condition of half-filling reads

$$\sum_{\sigma}\langle \hat{c}^{\dagger}_{i,\sigma}\hat{c}_{i,\sigma}\rangle = 1\ . \tag{6.6}$$

and thus fixes the number of electrons per site to one. On bipartite lattices this implies the invariance of the Hubbard Hamiltonian, $H = H_T + H_U$ under a particle-hole-transformation which is defined as

$$\hat{c}_{i,\sigma} \rightarrow \eta_i \hat{c}^{\dagger}_{i,-\sigma}\ , \tag{6.7}$$

with $\eta_i = \pm 1$ for $i \in A, B$. This takes $\hat{a}_{\uparrow}$ to $\hat{a}^{\dagger}_{\downarrow}$ and $\hat{b}_{\uparrow}$ to -$\hat{b}^{\dagger}_{\downarrow}$. The Green function $G_{\mathbf{k},\sigma}(\tau)$ is transformed like

$$\begin{aligned} G_{\mathbf{k},\sigma}(\tau) \quad &= \quad \frac{1}{N^2}\sum_{i,j}\langle \hat{c}_{i,\sigma}(\tau)\hat{c}^{\dagger}_{j,\sigma}\rangle e^{-\imath\mathbf{k}(i-j)} \\ &\overset{p-h-transf.}{=} \quad \eta_i\eta_j\frac{1}{N^2}\sum_{i,j}\langle \hat{c}^{\dagger}_{i,-\sigma}(\tau)\hat{c}_{j,-\sigma}\rangle e^{-\imath\mathbf{k}(i-j)} \end{aligned} \tag{6.8}$$

Thus, the Green function being a $2 \times 2$-matrix, acquires a minus sign only on the off-diagonal elements that is if $i$ and $j$ belong to different sublattices.
In short this means to study $\overline{G}_{\mathbf{k},\uparrow}(\tau) = \langle \hat{c}^{\dagger}_{\mathbf{k},\uparrow}(\tau)\hat{c}_{\mathbf{k},\uparrow}\rangle$ one only has to look at $G_{\mathbf{k},\downarrow}(\tau) = \langle \hat{c}_{\mathbf{k},\downarrow}(\tau)\hat{c}^{\dagger}_{\mathbf{k},,\downarrow}\rangle$.

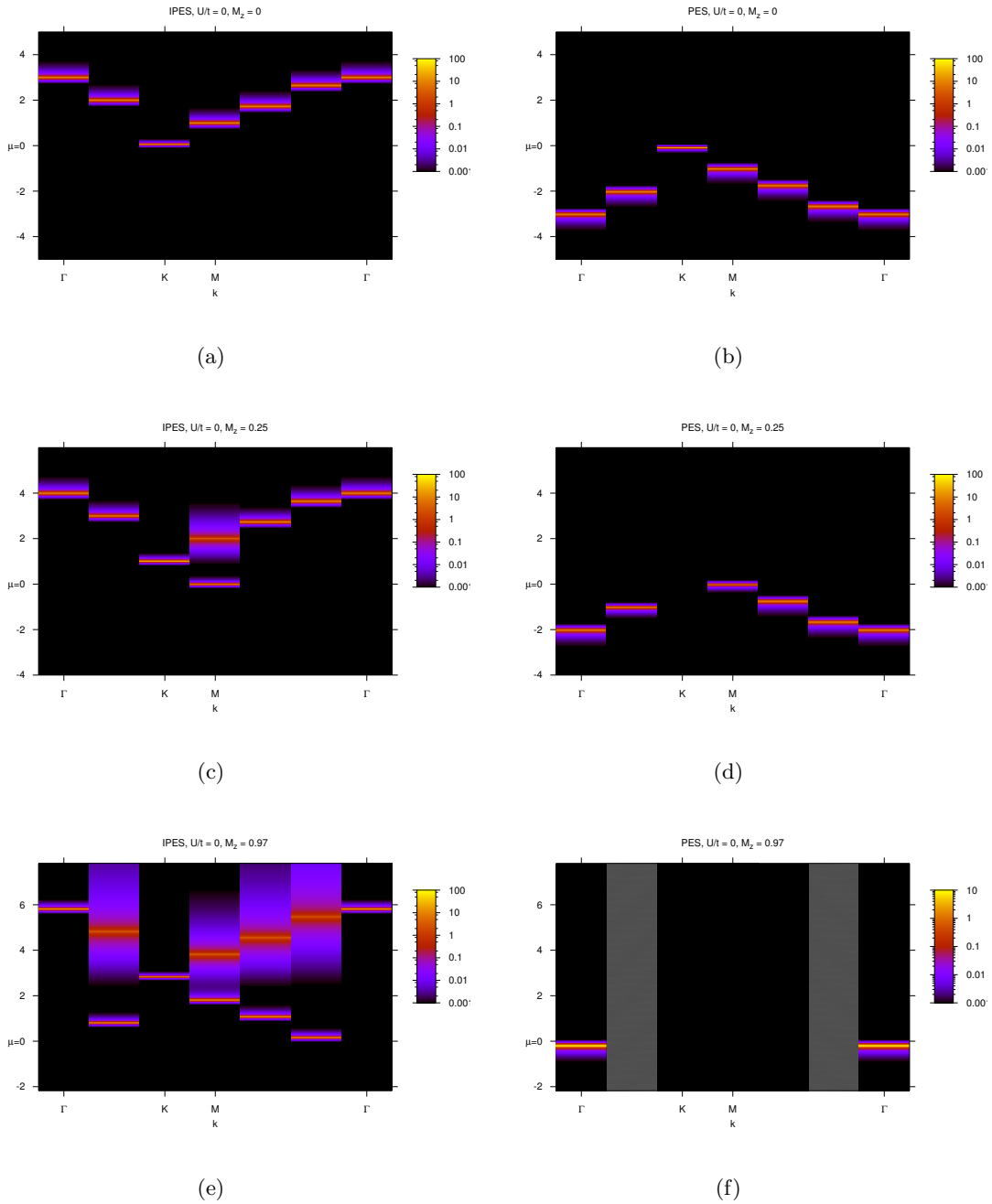


**Figure 6.3:** Single particle spectral function $A_{\uparrow,\uparrow}(\mathbf{k},\omega)$, the excitation spectra are labelled IPES and PES according to the experimental measurement. Owing to the discreteness of the $\mathbf{k}$-vectors the locus of the chemical potenial $\mu = 0$ can only be determined approximately.

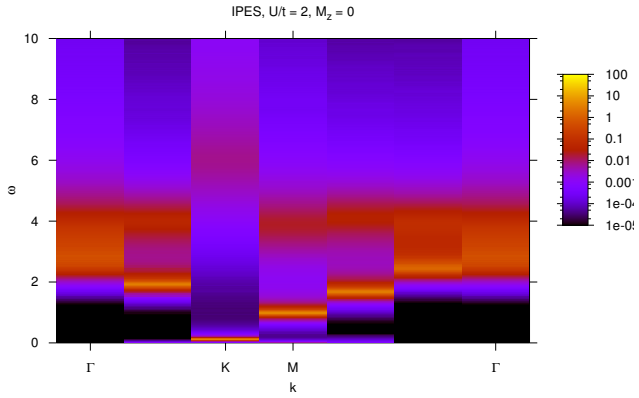


(a)

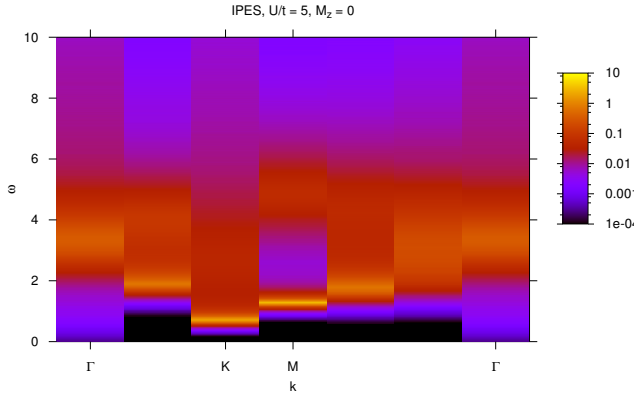


(b)

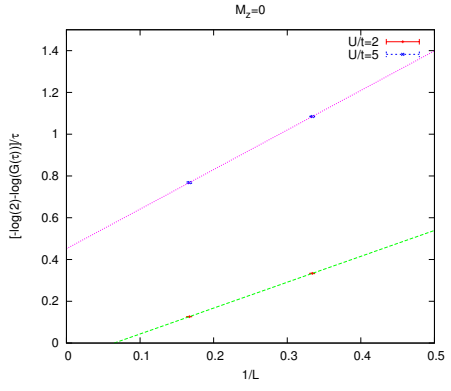


(c)

**Figure 6.4:** Single particle spectral function $A_{\uparrow,\uparrow}(\mathbf{k},\omega)$ below and beyond the critical interaction $U_c$. In order to estimate the influence of the finite-size effects, the energy gap (the excitation energy at $\mathbf{k} = \mathbf{K}$) was plotted as a function of inverse lattice size and linearly extrapolated to $1/L \to 0$. At $U = 5$ the gap stays finite in this limit ($f_{U=2}(x) = -0.08 + 1.24x$, $f_{U=5}(x) = -0.45 + 1.89x$).

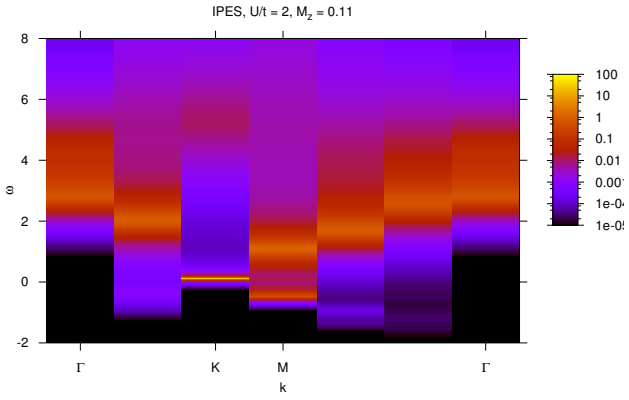


(a)

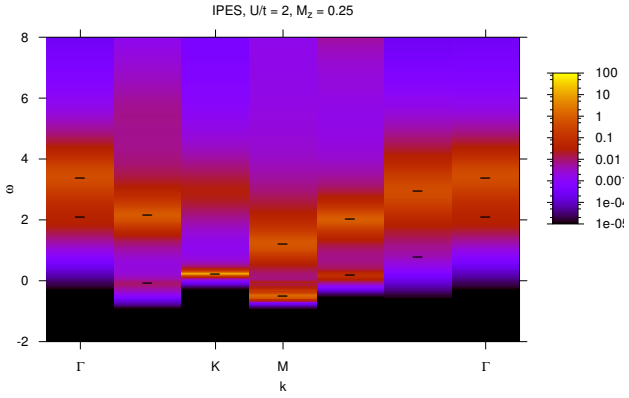


(b)

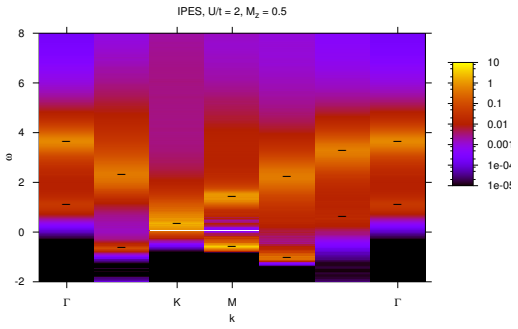


(c)

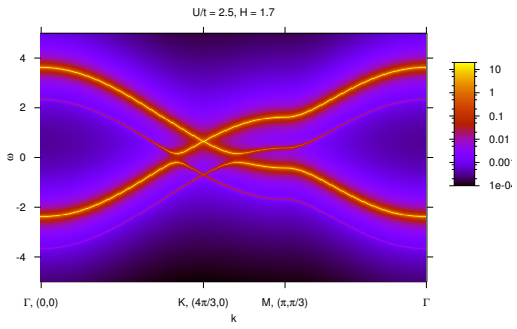


(d) Spectral function $A_{\uparrow,\uparrow}(\mathbf{k},\omega)$ as obtained from the mean field approximation (ch.2).

**Figure 6.5:** Single particle spectral function $A_{\uparrow,\uparrow}(\mathbf{k},\omega)$, from top to bottom the magnetization $M_z$ increases. Peaks of the spektral density are highlighted. We measure in the up-spin sector and for $M_z = 0.25$ and $M_z = 0.5$ one observes below the up-spin band weaker excitations which have dominatly down character due to the coupling of up and down-spin electrons. For comparison, the corresponding mean field data has been plotted. Since the chemical potential cannot be fixed without the corresponding PES measurements, the energy scale in Fig.(a)-(c) is just valid for relative comparisons.

As apparent from Fig.6.2, the single particle excitation spectra $A_{\uparrow,\uparrow}(\mathbf{k},\omega)$ display contributions which stem from the down spin sector. This can attributed to the electron-electron interaction which couples both sectors. In a simple picture, we understand this in terms of the propagation of a single up-spin electron which due to correlation effects picks up the dynamics of a down-spin electron.
This picture is consistent with the spectral functions we obtain in the mean field treatment 2.5. In the mean field approximation the excitation bands at different energies are however a direct consequence of the diagonalization of the mean-field Hamiltonian and we observe a similar distribution of the spectral weight.
In order to numerically prove the claim that an external magnetic field is inclined to open up a gap at the Fermi energy and thereby to lower the critical $U$, PES measurements of the spectral function for various magnetic fields would have to be carried out. This could not be accomplished within the time frame of this work.

# 7 Conclusion

The objective of this thesis was to study the ground state properties of the Hubbard model with a magnetic field term on the honeycomb lattice. This has been done using two approaches. First, we applied a mean field decoupling scheme to characterize the different phases of the system. We justified this approach by showing that the symmetry breaking phase transition to the canted antiferromagnetic state is a consequence of a Stoner like instability. We showed that the magnetic field generates a finite density of states at the Fermi energy and that nesting is present between the up and down spin Fermi surfaces. The transverse spin susceptibility diverges logarithmically and hence the critical value of $U$ at which the transition to the canted antiferromagnet occurs vanishes. The interplay between the magnetic field and the interaction strength was visualized in a phase diagram. The single-particle spectral function and the concomitant density of states were evaluated to demonstrate the opening and subsequent closing of the gap with increasing magnetic field.

In a second step, the system was studied using the projector quantum Monte Carlo (PQMC) approach [5]. The essential steps for the numerical treatment of the many-body problem were elucidated and include the path integral formulation of the partition function, the mapping of the electron-electron interaction to configurations of non-interacting Ising spins and the representation of the trial wave function as a Slater determinant. Via Wick's theorem which holds for a fixed configuration of the auxiliary field all observables can be reduced to Green functions. The zero-temperature time displaced Green function was implemented in a stable and efficient way in the pre-existing code (which had been written by F.F. Assaad) using a method suggested by M. Feldbacher and F.F. Assaad [35]. The numerical simulations go a good way in confirming the picture which emerges from the mean-field approximation. Although only lattices up to size $16 \times 16$ were considered and extrapolation to $1/L$ was only possible in a few cases, what one can establish quite rigorously is the existence of a magnetic ordered state above a critical $U_c$. Furthermore, the single particle excitation spectra which correspond to the experimental technique of inverse photoemission spectroscopy seem to suggest a close similarity to the mean field spectra. This makes us confident in claiming that already on the mean field level a good portion of the essential physics of the Hubbard model on the honeycomb lattice can be understood.

However, for a complete picture and in order to detect the opening of the gap at the Fermi

energy, spectral measurements corresponding to photoemission spectroscopy are needed. This, together with calculations at larger lattice sizes could be the subject of future research.

Finally, I would like to thank Fakher for guidance and teaching, Thomas for enlightening discussions and Jutta for reading the manuscript.

# Appendix

## A Lattice structure

The honeycomb (hexagonal) lattice has two atoms per unit cell and consists of two interpenetrating triangular sublattices $A$ and $B$. Two inequivalent Dirac points $K$ and $K\prime$ can be identified in the Brillouin zone, i.e. they are not connected by a linear combination of reciprocal lattice vectors.

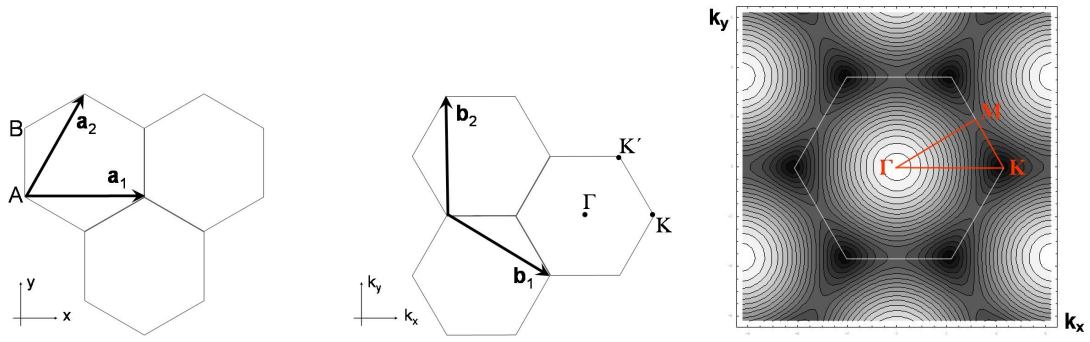


(a) Real space lattice vectors, $\mathbf{a}_1 = a\left(1, 0\right)$, $\mathbf{a}_2 = a\left(\frac{1}{2}, \frac{\sqrt{3}}{2}\right)$.

(b) Reciprocal space lattice vectors, $\mathbf{b}_1 = \frac{2\pi}{a}\left(1, -\frac{1}{\sqrt{3}}\right)$, $\mathbf{b}_2 = \frac{2\pi}{a}\left(0, \frac{2}{\sqrt{3}}\right)$. The two inequivalent Dirac points are denoted **K** and **K**$\prime$.

(c) Contour plot of the free dispersion relation, with the high symmetrie path of the first Brilloin zone, Γ-$K$-$M$-Γ.

**Figure .1:** Defintion of real and reciprocal lattice vectors of the honeycomb lattice.

Near each corner of the Brillouin zone the energy depends conically on the wave vector $\mathbf{k} = (k_x, k_y)$. The dispersion relation therefore is linear on the displacement $\delta\mathbf{k}$,

$$|E| = \hbar v_F |\delta\mathbf{k}| \; . \tag{.1}$$

This can be shown by a low-energy approximation of the tight binding Hamiltonian (2.3)

$$H_T = -t \sum_{\mathbf{k},\sigma} \begin{pmatrix} \hat{a}^\dagger_{\mathbf{k},\sigma} & \hat{b}^\dagger_{\mathbf{k},\sigma} \end{pmatrix} \begin{bmatrix} 0 & H_{12} \\ H_{21} & 0 \end{bmatrix} \begin{pmatrix} \hat{a}_{\mathbf{k},\sigma} \\ \hat{b}_{\mathbf{k},\sigma} \end{pmatrix} \; , \tag{.2}$$

with $H_{12} = H^*_{21}$. The following arguments are basically a summary of the references [28], [43] and [44]. Using standard notation we write down the Dirac points in a slightly different

way than indicated above, i.e. with the translation $\mathbf{K\prime} \rightarrow \mathbf{K\prime} - \Big(\mathbf{b}_1 + \mathbf{b}_2\Big)$. This results in $\mathbf{K}, \mathbf{K\prime} = \pm\frac{2\pi}{a}\Big(\frac{2}{3}, 0\Big)$ with $\Gamma \equiv \Big(0, 0\Big)$. We now expand $H_T$ around the two inequivalent points $\mathbf{K}$ and $\mathbf{K\prime}$ and subsequently obtain the linearized Hamiltonian $H_{Dirac} = H_{\mathbf{K}} + H_{\mathbf{K\prime}}$. To linear order a Taylor expansion around the $\mathbf{K}$-point gives

$$H_{12}(\mathbf{K}+\mathbf{k}) = \underbrace{H_{12}(\mathbf{K})}_{=0} - \frac{\sqrt{3}}{2}\, a\, \Big(k_x - \imath k_y\Big)\,. \tag{.3}$$

Thus,

$$H_{\mathbf{K}} = \frac{\sqrt{3}}{2}\, a\, t \sum_{\mathbf{k},\sigma} \begin{pmatrix} \hat{a}^\dagger_{\mathbf{k},\sigma} & \hat{b}^\dagger_{\mathbf{k},\sigma} \end{pmatrix} \begin{bmatrix} 0 & k_x - \imath k_y \\ k_x + \imath k_y & 0 \end{bmatrix} \begin{pmatrix} \hat{a}_{\mathbf{k},\sigma} \\ \hat{b}_{\mathbf{k},\sigma} \end{pmatrix}\,. \tag{.4}$$

The same procedure can be applied to the valley around $\mathbf{K\prime}$ leading to

$$H_{\mathbf{K\prime}} = \frac{\sqrt{3}}{2}\, a\, t \sum_{\mathbf{k},\sigma} \begin{pmatrix} \hat{a}^\dagger_{\mathbf{k},\sigma} & \hat{b}^\dagger_{\mathbf{k},\sigma} \end{pmatrix} \begin{bmatrix} 0 & -k_x - \imath k_y \\ -k_x + \imath k_y & 0 \end{bmatrix} \begin{pmatrix} \hat{a}_{\mathbf{k},\sigma} \\ \hat{b}_{\mathbf{k},\sigma} \end{pmatrix}\,. \tag{.5}$$

Upon diagonalization one gets the two branches

$$E(\mathbf{k}) = \pm\frac{\sqrt{3}}{2}\, a\, t \sqrt{k_x^2 + k_y^2}\,, \tag{.6}$$

which confirms (.1). Here the energy independent group velocity of the low-energy excitations $v_F = \frac{\sqrt{3}}{2\hbar}\, a\, t$ was defined.
The low energy excitations are therefore massless quasiparticles. In the following the correspondance of the low energy tight binding model to massless (2+1) dimensional QED will be shown. To proceed we introduce a spinor notation

$$\phi_{\mathbf{K}+\mathbf{k},\sigma} = \begin{pmatrix} \hat{a}_{\mathbf{K}+\mathbf{k},\sigma} \\ \hat{b}_{\mathbf{K}+\mathbf{k},\sigma} \end{pmatrix}\,. \tag{.7}$$

Since these spinors result from the two atomic unit cell of the lattice they are not related to electron spin but to "pseudospin" which discriminates between sublattice $A$ and $B$. Like real spin this degree of freedom is described by the Pauli matrices $\sigma_i$. We can write (.4) and (.6) as a two dimensional Dirac equation,

$$H_{Dirac} = H_{\mathbf{K}} + H_{\mathbf{K\prime}} = \sum_{\mathbf{k},\sigma} \phi^\dagger_{\mathbf{K}+\mathbf{k},\sigma} H_{\mathbf{K}} \phi_{\mathbf{K}+\mathbf{k},\sigma} + \phi^\dagger_{\mathbf{K\prime}+\mathbf{k},\sigma} H_{\mathbf{K\prime}} \phi_{\mathbf{K\prime}+\mathbf{k},\sigma}\,. \tag{.8}$$

In the above equation, we use the short notation

$$\begin{aligned} H_{\mathbf{K}} &= \hbar v_F \Big(\sigma_1 k_x + \sigma_2 k_y\Big) \\ H_{\mathbf{K\prime}} &= \hbar v_F \Big(-\sigma_1 k_x + \sigma_2 k_y\Big)\,. \end{aligned} \tag{.9}$$

In addition to the Pauli matrices $\sigma_i$ describing the sublattice degree of freedom one may use a second set of Pauli matrices $\tau_i$ acting in the valley $(\mathbf{K}, \mathbf{K}\prime)$ subspace. To arrive at a compact notation we introduce the four-component spinor $\Psi_{\mathbf{k},\sigma}$,

$$\Psi_{\mathbf{k},\sigma} = \begin{pmatrix} \Psi_{\mathbf{K}+\mathbf{k},\sigma} \\ \Psi_{\mathbf{K}\prime+\mathbf{k},\sigma} \end{pmatrix} = \begin{pmatrix} \hat{a}_{\mathbf{K}+\mathbf{k},\sigma} \\ \hat{b}_{\mathbf{K}+\mathbf{k},\sigma} \\ \hat{b}_{\mathbf{K}\prime+\mathbf{k},\sigma} \\ \hat{a}_{\mathbf{K}\prime+\mathbf{k},\sigma} \end{pmatrix} . \tag{.10}$$

Defining the $4 \times 4$ matrices $\alpha_{1,2}$ [44] as

$$\alpha_{1,2} = \tau_3 \otimes (\sigma_1, \sigma_2) = \begin{pmatrix} \sigma_1 & 0 \\ 0 & -\sigma_1 \end{pmatrix} , \begin{pmatrix} \sigma_2 & 0 \\ 0 & -\sigma_2 \end{pmatrix} , \tag{.11}$$

the Hamiltonian (.8) reads

$$H_{Dirac} = \hbar v_F \sum_{\mathbf{k},\sigma} \Psi^{\dagger}_{\mathbf{k},\sigma} H_{\mathbf{k}} \Psi_{\mathbf{k},\sigma} \ , \ H_{\mathbf{k}} = \alpha_1 k_x + \alpha_2 k_y \ . \tag{.12}$$

One may also write

$$H_{\mathbf{k}}\Psi = E\Psi \ , \ H_{\mathbf{k}} = v_F \Big( \mathbf{k} \cdot \sigma \Big) \otimes \tau_3 \ . \tag{.13}$$

Summarizing the above results, the quasiparticles on the honeycomb lattice are at low energies accurately described by the $(2+1)$ dimensional Dirac equation. The effective speed of light is $v_F \approx 10^6 m/s$. To conclude with, based on topological arguments the Dirac cone can be shown to be stable against third neighbour (i.e diagonal) hopping, characterized by $t\prime$ as long as $-3 \leq t\prime/t < 1$ is satisfied [44]. As the same authors point out, the appearence of gapless Dirac fermions is not limited to the honeycomb lattice and is a generic feature of a class of two dimensional lattices which interpolate between square $(t\prime = t)$ and $\pi$-flux $(t\prime = -t)$ lattices.

# B Singular Value Decompostion

SDV is a technique which deals with matrices that are either singular or else numerically very close to singular [9]. Its based on a theorem of linear algebra which states that any matrix $\mathbf{A}$ $(M \times N, M \geq N)$ can be written as the matrix product of a column-orthogonal matrix $\mathbf{U}$ $(M \times N)$, a diagonal matrix $\mathbf{D}$ $(N \times N)$ and the transpose of an orthogonal

matrix $\mathbf{V}$ $(N \times N)$:

$$\begin{pmatrix} & & \\ & \mathbf{A} & \\ & & \end{pmatrix} = \begin{pmatrix} & & \\ & \mathbf{U} & \\ & & \end{pmatrix} \cdot \begin{pmatrix} d_1 & & \\ & \cdots & \\ & & d_N \end{pmatrix} \begin{pmatrix} & & \\ & \mathbf{V}^T & \\ & & \end{pmatrix} . \tag{.14}$$

The diagonal matrix $\mathbf{D}$ contains the scales $d_1 \cdots d_N$: positive or (numerically close to) zero elements. The orthogonalization routine can be understood intuitively using the familiar Gram-Schmidt orthonormalization method, but the actual decompostion as we use is based on the Householder algorithm. This technique is more stable and is extensively discussed in [9].

# C Metropolis scheme

The Metropolis algorithm is based on the assumption that a simulated thermodynamic system changes its configuration from energy $E_1$ to energy $E_2$ with probability $p = e^{-(E_2-E_1)/k_BT}$ in agreement with the Boltzmann probability distribution [9]. In the case of $E_2 > E_1$ the probability $p$ to change is smaller than unity and this option is accepted according to this probability. The decision to accept/reject the move in that case is made by generating a random number $r$ between zero and unity: the move is accepted if $r < p$ and rejected otherwise. In the opposite situation $E_2 < E_1$ the move is automatically accepted. More compactly this strategy can be written as

$$p_{acceptance}(old \to new) = \min\Big(1, p\Big) . \tag{.15}$$

As described in section 5.1.1, the decision to move from a given configuration of auxilliary fields $\mathbf{s}$ to a new configuration $\mathbf{s\prime}$ with one Ising spin being flipped is governed by the ratio (5.12)

$$R = \frac{P_{\mathbf{s\prime}}}{P_{\mathbf{s}}} . \tag{.16}$$

Thus, the proposed change is accepted with probability

$$p_{acceptance}(\mathbf{s} \to \mathbf{s\prime}) = \min\Big(1, R\Big) . \tag{.17}$$

# D Approximation of $\tanh(x)$

In order to evaluate the antiferromagnetic susceptibility $\chi_{AFM}$ the following approximation for $\tanh(x)$ is used which amounts to a linearization around $x = 0$ is used:

$$\tanh(x) = \left\{ \begin{array}{ll} x, & |x| < 1 \\ 1, & x > 1 \\ -1, & x < -1 \end{array} \right\} \tag{.18}$$

$$\begin{aligned} \chi^{+-}_{\mu\mu} - \chi^{+-}_{\mu\nu} &= \frac{1}{2} \sum_{j=\gamma,\eta} \frac{1}{N} \sum_{\mathbf{k}} \frac{1}{2\xi_j} \tanh\left(\frac{\beta}{2}\xi_j\right) \\ &= \frac{1}{2} \sum_{j=\gamma,\eta} \int d\xi_j DOS(\xi_j) \frac{1}{2\xi_j} \tanh\left(\frac{\beta}{2}\xi_j\right) \\ &= \frac{1}{2} \sum_{j=\gamma,\eta} \left[ \int_{-2/\beta}^{+2/\beta} d\xi_j \frac{\beta}{2}\xi_j + \int_{+2/\beta}^{W} d\xi_j - \int_{-W}^{-2/\beta} d\xi_j \right] DOS(\xi_j) \frac{1}{2\xi_j} \\ &\approx \frac{1}{2} \sum_{j=\gamma,\eta} DOS(\epsilon_{F,j}) \left[ \int_{+2/\beta}^{W} d\xi_j - \int_{-W}^{-2/\beta} d\xi_j \right] \frac{1}{2\xi_j} \\ &= \frac{1}{2} \sum_{j=\gamma,\eta} DOS(\epsilon_{F,j}) \ \ln\left(\frac{W}{2T}\right) \end{aligned} \tag{.19}$$

In line three we introduced the bandwidth $W$ and approximated the density of states with the density of states at the fermi level, $DOS(\xi_j) \approx DOS(\epsilon_{F,j})$.

# Bibliography


[1] J.W.Negele, H.Orland, *Quantum Many-Particle Systems* (Westview Press, Boulder, 1989)

[2] P.Fazekas, *Lecture Notes on Electron Correlation and Magnetism* (World Scientific, Singapore, 1999)

[3] W.Nolting, *Grundkurs Theoretische Physik 7, Viel-Teilchen-Theorie* (Springer, Berlin, Heidelberg, 2005)

[4] H.Bruus,K.Flensberg, *Many-Body Quantum Theory in Condensed Matter Physics* (Oxford University Press, Oxford, 2004)

[5] F.F.Assaad, H.G.Evertz, *World-line and Determinental Quantum Monte Carlo Methods* (in H.Fehske, R.Schneider, A.Weiße (Eds.), *Computational Many-Particle Physics*) (Springer, Berlin, Heidelberg, 2008)

[6] F.F.Assaad, *Quantum Monte Carlo Methods on Lattices: The Determinental Approach* (in J.Grotendorst, D.Marx, A.Muramatsu (Eds.), *Quantum Simulations of Complex Many-Body Systems: From Theory to Algorithms*) (NIC, Jülich, 2002)

[7] X.-G.Wen, *Quantum Field-Theory of Many-Body Systems* (Oxford University Press, Oxford, 2004)

[8] M.E.Peskin, D.V.Schroeder, *An Introduction to Quantum Field Theory* (Westview Press, Boulder, 1995)

[9] W.H.Press et al., *Numerical Recipes in C* (Cambridge University Press, Cambridge, 1997)

[10] S.V.Morozov et al., Phys. Rev. Lett., **100**, 016602 (2008)

[11] E.Zhao, A.Paramekanti, Phys. Rev. Lett. **97**, 230404 (2006)

[12] T.Ohta et al., Phys. Rev. Lett., **98**, 206802 (2007)

[13] S.Sorella, E.Tosatti, Europhys. Lett., **19**, 699 (1992)

[14] N.M.R.Peres, Phys. Rev. B, **70**, 195122 (2004)

[15] N.M.R.Peres, Phys. Rev. B, **72**, 174406 (2005)

[16] T.Paiva et al., Phys. Rev. B, **72**, 085123 (2005)

[17] S.Saremi, P.A.Lee, Phys. Rev. B, **75**, 165110 (2007)

[18] J.C.Slonczewski, P.R.Weiss, Phys. Rev., **109**, 272 (1958)

[19] S.Das Sarma et al., Phys. Rev. B, **75**, 121406(R) (2007)

[20] G.W.Semenoff, Phys. Rev. Lett., **53**, 2449 (1984)

[21] C.Honerkamp, *Density waves and Cooper pairing on the honeycomb lattice*, URL `http://arxiv.org/abs/cond-mat/0711.1259v1`

[22] N.Furukawa, *Antiferromagnetism of the Hubbard model on a layered Honeycomb lattice - Is MgB2 a nearly-antiferromagnetic metal?*, URL `http://arxiv.org/abs/cond-mat/0103184v3`

[23] G.Baskaran, S.A.Jafari, Phys. Rev. Lett., **89**, 016402 (2002)

[24] H.P.Dahal et al., Phys. Rev. B, **74**, 233405 (2006)

[25] H.P.Dahal et al., URL `http://arxiv.org/abs/cond-mat/0706.1689v1`

[26] I.F.Herbut, Phys. Ref. Lett., **97**, 146401 (2006)

[27] S.Saremi, URL `http://arxiv.org/abs/cond-mat/0705.0187v2`

[28] A.K.Geim, K.S.Novoselov, Nature Materials, **6**, 183 (2007)

[29] A.Bostwick et al., Nature Physics, **3**, 36 (2007)

[30] S.Y.Zhou et al., Nature Physics, **2**, 595 (2006)

[31] K.S.Novoselov, Nature Letters, **483**, 197 (2005)

[32] M.I.Katsnelson et al., Nature Physics, **2**, 620 (2006)

[33] F.Schedin, Nature Materials, **6**, 652 (2007)

[34] S.Pisana, Nature Materials, **6**, 198 (2007)

[35] M.Feldbacher, F.F.Assaad, Phys. Rev. B, **63**, 073105, 2001

[36] R.M.Fye, Phys. Rev. B, **33**, 6271 (1986)

[37] J.E.Hirsch, Phys. Rev. B, **28**, 4059 (1983)

[38] R.R. dos Santos, Braz. J. Phys., **33**, 36 (2003)

[39] T.C. Lang, Diploma thesis (TU Graz, Graz, 2005)

[40] K.S.D.Beach, *Identifying the maximum entropy method as a special limit of stochastic analytic continuation.* URL `http://arxiv.org/abs/cond-mat/0403055`

[41] A.W.Sandvik,Phys. Rev. B **57**, 10287 (1998)

[42] R.N.Silver, D.S.Sivia, J.E.Gubernatis, Phys. Rev. B, **41**, 2380 (1990)

[43] C.W.J.Beenakker, *Andreev reflection and Klein tunneling in graphene*, URL `http://arxiv.org/abs/cond-mat/0710.3848v2`

[44] V.P.Gusynin, S.G.Sharapov, J.P.Carbotte, *AC conductivity of graphene: from tight-binding model to 2+1-dimensional quantum electrodynamics*, URL `http://arxiv.org/abs/cond-mat/0706.3016v2`

# Erklärung

Ich versichere hiermit, daß ich die vorgelegte Diplomarbeit am Institut für Theoretische Physik und Astrophysik der Julius-Maximillians-Universität Würzburg unter der Anleitung von Prof. Dr. F. F. Assaad selbständig durchgeführt und keine anderen Quellen und Hilfsmittel als die angegebenen benutzt habe.

Würzburg, 14. April 2008

Martin Bercx